ACS OMEGA

http://pubs.acs.org/journal/acsodf

Article

# Adsorption–Desorption Behavior of Arsenate Using Single and Binary Iron-Modified Biochars: Thermodynamics and Redox Transformation

Md. Aminur Rahman,* Dane Lamb, Mohammad Mahmudur Rahman, Md Mezbaul Bahar, and Peter Sanderson

Cite This: *ACS Omega* 2022, 7, 101–117

Read Online

ACCESS | Metrics & More | Article Recommendations | Supporting Information

**ABSTRACT:** Arsenic (As) is a dangerous contaminant in drinking water which displays cogent health risks to humans. Effective clean-up approaches must be developed. However, the knowledge of adsorption–desorption behavior of As on modified biochars is limited. In this study, the adsorption–desorption behavior of arsenate ($As^V$) by single iron (Fe) and binary zirconium–iron (Zr–Fe)-modified biosolid biochars (BSBC) was investigated. For this purpose, BSBC was modified using Fe-chips (FeBSBC), Fe-salt ($FeCl_3$BSBC), and Zr–Fe-salt (Zr–$FeCl_3$BSBC) to determine the adsorption–desorption behavior of $As^V$ using a range of techniques. X-ray photoelectron spectroscopy results revealed the partial reduction of pentavalent $As^V$ to the more toxic trivalent $As^{III}$ form by $FeCl_3$BSBC and Zr–$FeCl_3$BSBC, which was not observed with FeBSBC. The Langmuir maximum $As^V$ adsorption capacities were achieved as 27.4, 29.77, and 67.28 mg/g when treated with FeBSBC (at pH 5), $FeCl_3$BSBC (at pH 5), and Zr–$FeCl_3$BSBC (at pH 6), respectively, using 2 g/L biochar density and 22 ± 0.5 °C. Co-existing anions reduced the $As^V$ removal efficiency in the order $PO_4^{3-} > CO_3^{2-} > SO_4^{2-} > Cl^- > NO_3^-$, although no significant inhibitory effects were observed with cations like $Na^+$, $K^+$, $Mg^{2+}$, $Ca^{2+}$, and $Al^{3+}$. The positive correlation of $As^V$ adsorption capacity with temperature demonstrated that the endothermic process and the negative value of Gibbs free energy increased (−14.95 to −12.47 kJ/mol) with increasing temperature (277 to 313 K), indicating spontaneous reactions. Desorption and regeneration showed that recycled Fe-chips, Fe-salt, and Zr–Fe-salt-coated biochars can be utilized for the effective removal of $As^V$ up to six-repeated cycles.

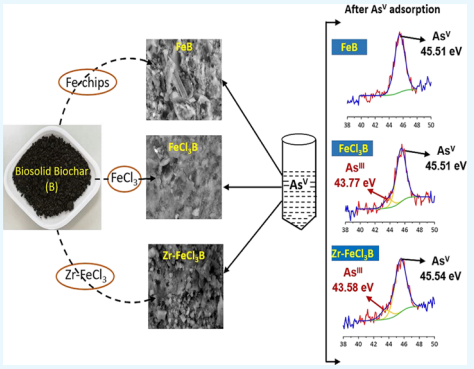


## 1. INTRODUCTION

Arsenic (As) is included as a group 1 carcinogenic chemical[1] which occurs naturally in the Earth's groundwater. Natural sources such as weathering and dissolution of As-enriched minerals, volcanic emissions, and biological reactions and anthropogenic sources like mining and smelting operations, wood preservation activities, pesticides use in agriculture, and discharge from tannery and battery industries, all make major contributions to the release of As into the environment.[2−4] The As in water is commonly present as inorganic oxyanions of trivalent arsenite ($AsO_3^{3-}$ and $As^{3+}$) and pentavalent arsenate ($AsO_4^{3-}$ and $As^{5+}$).[2,5,6] It is reported that more than 200 million people in 107 countries are adversely affected by a range of health-related issues caused by the consumption of elevated levels of As-tainted drinking water greater than the World Health Organization (WHO) provisional guideline value of 10 μg/L.[7,8] Chronic exposure to As can cause cancer of the bladder, skin, and lungs and other impacts to the central nervous system, IQ impacts in children, skin pigmentation, cardiovascular systems, hypertension, and endocrine disruption.[9−11] Therefore, an efficient As removal technology from water is paramount to protect human health and the environment.

Over the last few decades, various removal strategies such as oxidation, precipitation/co-precipitation, coagulation, ion exchange, reverse osmosis, membrane separation techniques, and adsorption have served to either remove or diminish As concentrations below the WHO provisional guideline value.[12−19] Among these options, adsorption is one of the efficient techniques for the removal of As from contaminated water as this technique is simple, cost-effective, and produces less waste products.[20−22] Various adsorbents such as clay, modified clay, and clay supported nano zero valent iron (nZVI),[23−26] alumina,[27−29] activated carbon,[30−32] graphene,[33]

Received: August 2, 2021
Accepted: December 23, 2021
Published: January 3, 2022

© 2022 The Authors. Published by American Chemical Society

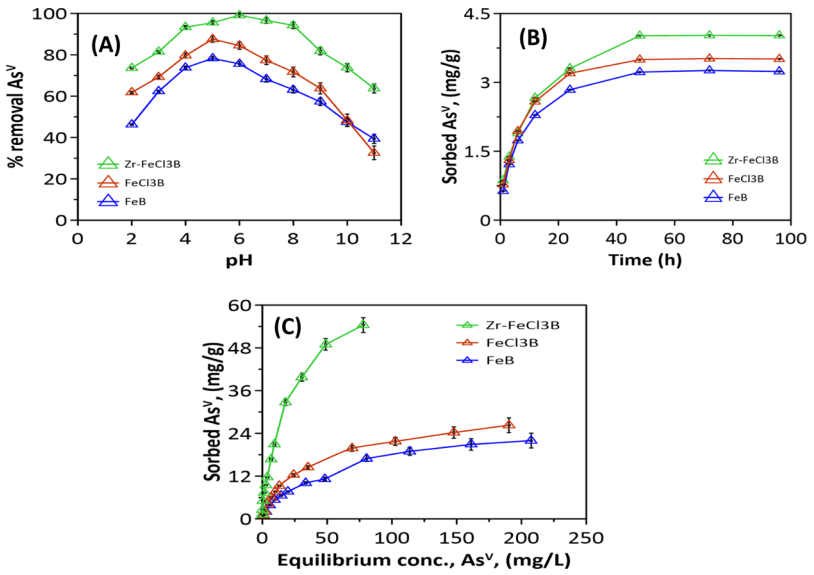


**Figure 1.** (A) Effect of pH on removal (%) of $As^V$, (B) effect of time on adsorption capacity of $As^V$ (initial $As^V$ concentration was 10 mg/L, BC dosage was 2 g/L, and temperature was 22 °C), and (C) adsorption capacity at equilibrium of FeB, $FeCl_3B$ (pH 5), and Zr−$FeCl_3B$ at pH 6 (initial $As^V$ concentration was 5−300 mg/L, BC density was 2 g/L, pH was 5 for FeB and $FeCl_3B$, pH was 6 for Zr−$FeCl_3B$, and temperature was 22 ± 0.5 °C).

and biochar (BC)[34−36] have been used to remove As from contaminated waters.

In contrast to activated carbon, BC has emerged as an affordable remediation substrate for the removal of environmental pollutants in natural and wastewaters.[37−40] However, the adsorption efficiency of pristine BCs can be improved by single or binary metal loadings on to BC surfaces.[41−46] Natural and synthetic Fe (hydr)oxides and Fe-based materials are promising to remove As from aqueous solutions effectively.[47−50] Iron-based adsorbents are commonly being used for remediation techniques because (1) generally, these adsorbents are relatively favorable to As adsorption and are environmentally friendly[51,52] and (2) As is mostly co-precipitated with Fe, and the As-removal efficiency depends on the Fe/As ratio during co-precipitation.[53,54] Superior As removal efficiency was reported by the higher Fe/As ratio.[55,56] However, As mobilization is controlled by pH, oxidation number, and elements like Fe and Mn.[49,57,58]

Several studies have demonstrated that strong adsorption of As occurs from aqueous solution on the surface of binary metal oxides including Fe−Al,[59] Fe−Cu,[60] Fe−Mn,[49,61,62] Fe−Ni,[63,64] and Fe−Zr.[65] In recent years, utilization of bimetals such as zirconium (Zr) and Fe for the modification of BC exhibits a much higher adsorption capacity for $As^V$ compared to individual Fe- and Zr-modified BC.[46] Very limited study has been reported on the removal of $As^V$ using Zr−Fe-modified BC.[46] In addition, Ren et al. (2011) reported the high adsorption capacity of the Fe−Zr binary oxide adsorbent in removing both $As^V$ and $As^{III}$ from water.[66] Additionally, the practical application of adsorbents in removing As can be evaluated by desorption and reusability testing. After performing As adsorption, adsorbents in the suspension are needed to be regenerated using acids or alkali to evade secondary contamination. Therefore, additional management is required to minimize the risk of regenerated As-containing solutions before disposal.[67,68]

Under oxic environments, BC may potentially reduce $As^V$ to $As^{III}$ by donating electrons from the surface of BC.[14,69] It was reported that partial reduction of $As^V$ occurred on the BC surface under oxic conditions with BC produced at 300 and 700 °C, respectively.[14] Nevertheless, the redox transformation of $As^V$ and the bonding chemistry by modified BCs are still largely unexplored. Hence, it is crucial to investigate adsorption−desorption behavior of $As^V$ by bimetal (Fe and Zr)-modified BC and to explore whether modified BC reduces $As^V$ to $As^{III}$ during adsorption. However, there is little evidence in the literature that modified BCs may lead to $As^V$ reduction. Thus, additional research is required to investigate the modification of BCs using single Fe and Zr−Fe bimetals for the removal of As from aqueous solutions.

The aims of the current study were to (1) synthesize Fe-coated BCs from two different commercial Fe-sources using metallic Fe-chips and Fe-salt ($FeCl_3{\cdot}6H_2O$); (2) synthesize additional Zr−$FeCl_3$-coated BC to assess the affinity of Zr−Fe bimetals on As binding;[65,70] (3) examine the adsorptive behavior of Fe in the presence of Zr; (4) evaluate the effectiveness of single and binary Fe- and Zr−$FeCl_3$-coated BCs in removing $As^V$ from aqueous solution using batch experiments; (5) explore the redox transformation of sorbed $As^V$ on the BC surface by XPS; and (6) undertake a desorption study of As-loaded BCs for assessing regeneration and stability in practical applications of these adsorbents.

## 2. RESULTS AND DISCUSSION

**2.1. $As^V$ Adsorption Experiments in Single Fe and Binary Zr−Fe-Modified BCs.** *2.1.1. Solution pH.* The adsorption process is greatly affected by the pH-dependent surface protonation and deprotonation of metal oxide/hydroxides. First, protonation of the metal hydroxide surfaces occurs at low pH (pH < 5), and the deprotonation of metal hydroxide tends to increase with increasing pH (pH > 7). This result is due to the low affinity among oxyanions of As-species and adsorbents at high solution pH.[66,71−73] Figure 1A displays the percentage of $As^V$ (10 mg/L) removal by all examined Fe-modified BCs. Figure 1A describes that the amount of adsorbed $As^V$ sharply increased up to pH 5 and then gradually


https://doi.org/10.1021/acsomega.1c04129
ACS Omega 2022, 7, 101−117

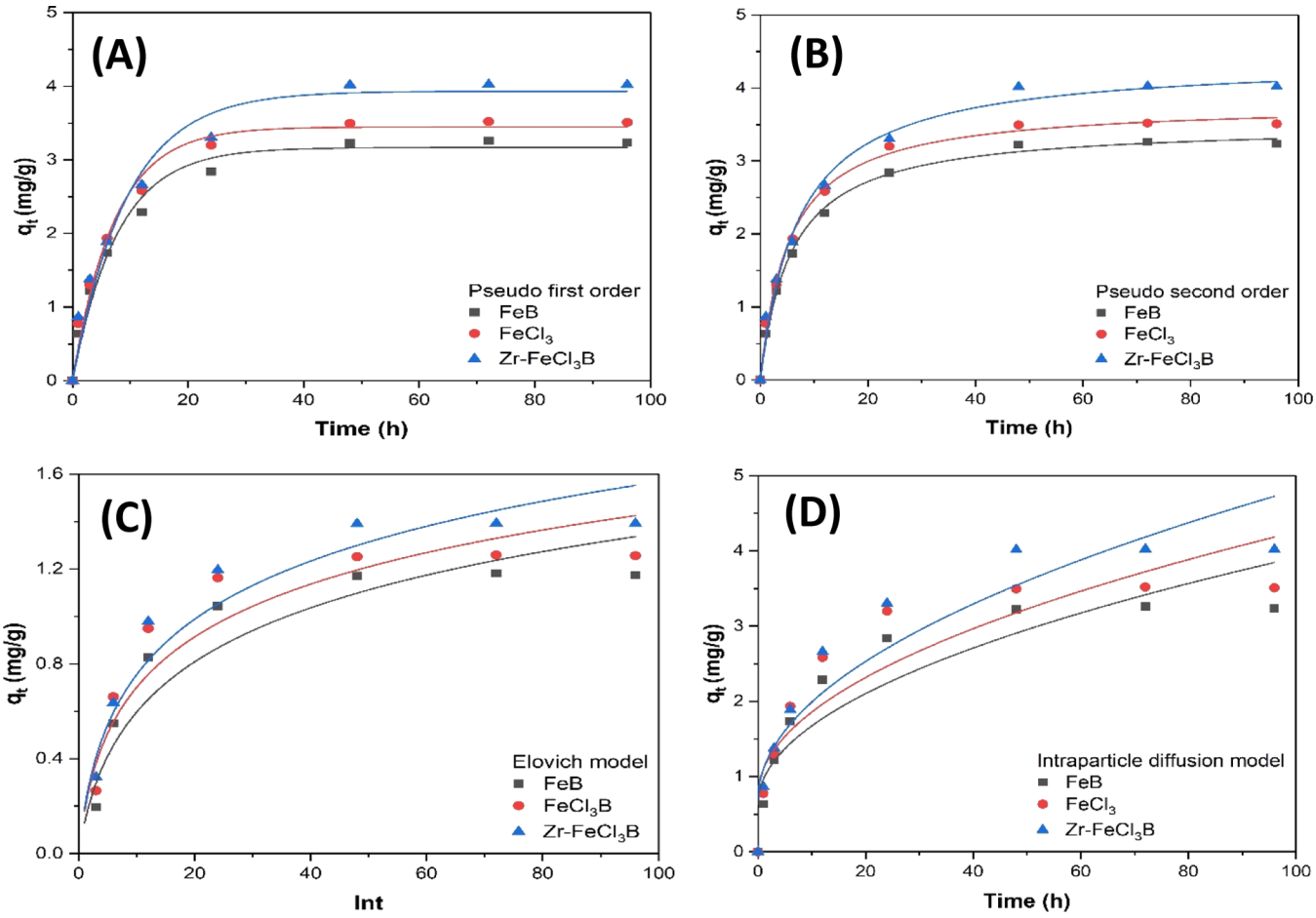


**Figure 2.** Non-linear kinetic models: pseudo-first-order (A), pseudo-second-order (B), Elovich (C), and intraparticle diffusion model (D) (initial $As^V$ concentration was 10 mg/L, BC density was 2 g/L, and pH was 6 at 22 ± 0.5 °C).

**Table 1. Kinetic Models and Best−Fit Parameters for $As^V$ Adsorption Data**

| | | pseudo-first-order | | | pseudo-second-order | | | Elovich | | | intraparticle diffusion | | | |
|---|---|---|---|---|---|---|---|---|---|---|---|---|---|---|
| BC | $q_{e\text{-}exp}$ (mg/g) | $k_1$ (1/h) | $q_{e\text{-}cal}$ | $R^2$ | $k_2$ (g/mg/h) | $q_{e\text{-}cal}$ (mg/g) | $R^2$ | $\beta$ (mg/g) | $\alpha$ (mg/g h) | $R^2$ | $k_{id}$ (g/mg/$h^{1/2}$) | C (mg/g) | $R^2$ | pH |
| FeB | 3.26 | 0.12 | 3.16 | 0.98 | 0.05 | 3.50 | 0.99 | 2.81 | 0.15 | 0.81 | 0.33 | 0.64 | 0.85 | 5 |
| $FeCl_3B$ | 3.50 | 0.13 | 3.44 | 0.98 | 0.05 | 3.79 | 0.99 | 2.96 | 0.23 | 0.85 | 0.35 | 0.75 | 0.83 | 5 |
| Zr−$FeCl_3B$ | 4.02 | 0.11 | 3.93 | 0.97 | 0.03 | 4.39 | 0.99 | 2.67 | 0.24 | 0.91 | 0.41 | 0.68 | 0.89 | 6 |

decreased with further increasing pH from 6 to 11 for both FeB and $FeCl_3B$. Similarly, for Zr−$FeCl_3B$, $As^V$ adsorption increased up to pH 6 and then declined. The decreased adsorption at pH > 7 was due to the electrostatic repulsion of negatively charged $As^V$ species, ligand displacement from hydroxide, and the negative surface charge of adsorbents.[74]

The zeta potentials of FeB and $FeCl_3B$ were positive in the pH range of 2−4, with a net zeta potential value of +22.4 to +9.34 mV at pH 2−4 and +12.23 to +7.66 mV at pH 2−4, respectively. The zeta potential decreased gradually with increasing pH. The Zr−$FeCl_3$ coating possessed a net zeta potential of +25.02 mV at pH 2, decreasing to +4.78 mV at pH 6 (Table S1 in Supporting Information section). The point of zero charge ($pH_{PZC}$) for FeB, $FeCl_3B$, and Zr−$FeCl_3B$ were calculated as being 4.7, 4.9, and 6.3, respectively (Table S2 and Figure S1), which indicated that the BCs contained a net positive surface charge at pH < $pH_{PZC}$. At low pH, the BC composites performed as weak acids and formed positive surface sites that were able to attract negatively charged As species, such as $H_2AsO_4^-$, $HAsO_4^{2-}$, and $AsO_4^{3-}$. In addition, As adsorption was inhibited by electrostatic repulsion at high pH.[75] Similar findings have been reported by other studies for the adsorption of multi-protonated As species and other oxyanions such as $Cr^{VI}$ toward metal oxides and bio-adsorbents.[46,75−77]

*2.1.2. Reaction Time and Kinetic Modeling.* Adsorption kinetics is critical to determine the efficacy and mechanisms of adsorbate removal processes. The maximum $As^V$ removal efficiencies of FeB, $FeCl_3B$, and Zr−$FeCl_3B$ were 78.25 (at pH 5), 87.57 (at pH 5), and 99.15% (at pH 6), respectively, after 48 h (the initial concentration of $As^V$ was 10 mg/L). Virtually no further change was observed after this time (Figure 1B). Thus, $As^V$ adsorption remained constant after 48 h reaction time. To determine the reaction rate-controlling step for $As^V$ adsorption by Fe-coated BCs, four models were applied, including the pseudo-first-order, pseudo-second-order, Elovich model, and intraparticle diffusion model (Figure 2). The fitting parameters of the models are described in Table 1.



https://doi.org/10.1021/acsomega.1c04129
ACS Omega 2022, 7, 101−117

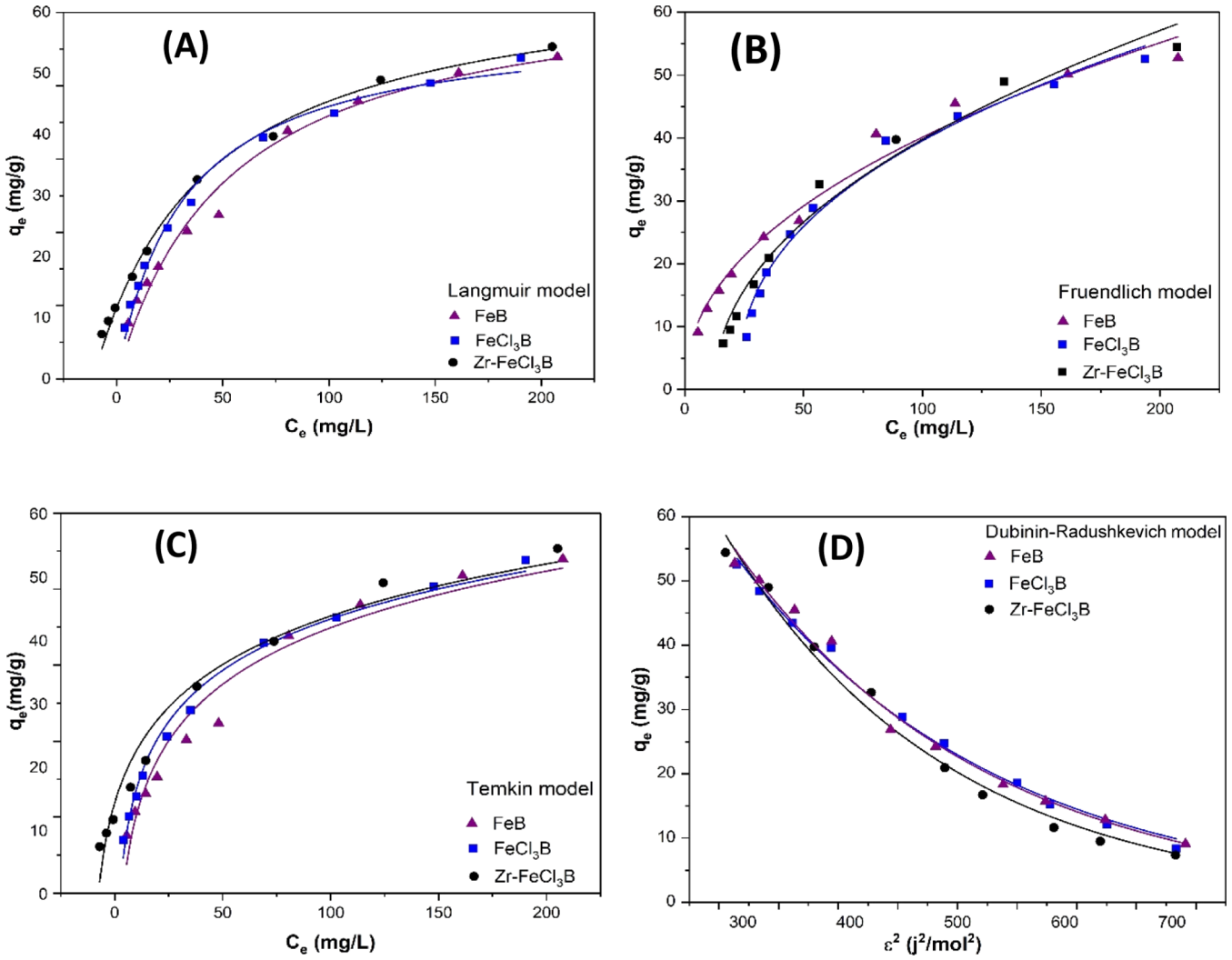


**Figure 3.** Non-linear fitting of isotherm models: Langmuir (A), Freundlich (B), Temkin (C), and D-R (D) (the initial $As^V$ concentration was 5−300 mg/L, BC density was 2 g/L, pH was 6, and temperature was 22 ± 0.5 °C).

The calculated $As^V$ adsorption capacity ($q_{e\text{-cal}}$) of FeB, $FeCl_3B$, and Zr−$FeCl_3B$ was 3.16, 3.44, and 3.93 mg/g, which is lower compared to the experimental value ($q_{e\text{-exp}}$) of 3.26, 3.5, and 4.02 (Table 1). The regression coefficient ($R^2$) values were 0.98, 0.98, and 0.97 of FeB, $FeCl_3B$, and Zr−$FeCl_3B$, respectively, for the pseudo-first-order kinetic model (Table 1). However, the regression coefficients ($R^2$) are closer to unity ($R^2$ = 0.99) for pseudo-second-order reaction kinetics (Table 1 and Figure 2B). The higher regression coefficient value ($R^2$ = 0.99) indicating the $As^V$ adsorption process was best fitted with the pseudo-second-order kinetic model (Table 1). Furthermore, the calculated $q_{e\text{-cal}}$ values were 3.5, 3.79, and 4.39 mg/g, which agreed well with the experimental $q_{e\text{-exp}}$ values for $As^V$ adsorption by FeB, $FeCl_3B$, and Zr−$FeCl_3B$ (Table 1). Thus, $As^V$ adsorption is mainly affected by chemical interactions between $As^V$ and the BC surface.

*2.1.3. Influence of Initial As-Concentration and Adsorption Isotherms.* Experimental adsorption data showed that the amount of $As^V$ adsorption increased when the $As^V$ concentration also increased (Figure 1C). However, $As^V$ removal efficiency gradually declined at high initial $As^V$ concentrations. This is because of the higher concentration difference between the adsorbents and the solution and the potential energy driving force.[75] In addition, the available active sites were fixed for Fe- and Zr−Fe-modified BCs, which would be saturated by $As^V$ at higher concentrations.

To evaluate the $As^V$ adsorption capacity of the single Fe-coating and binary Fe and Zr coatings BC, four adsorption isotherm models [Langmuir, Freundlich, Temkin, and Dubinin-Radushkevich (D-R)] were employed to fit the equilibrium adsorption data (Figure 3). The $R^2$ values ranged from 0.98−0.99, 0.98−0.98, 0.96−0.99, and 0.99−0.99 for the Langmuir, Freundlich, Temkin, and D-R models, respectively (Table 2). The maximum $As^V$ adsorption capacities achieved were 27.4, 29.77, and 67.28 mg/g by the Langmuir non-linear model fitting for FeB, $FeCl_3B$, and Zr−$FeCl_3B$, respectively (Table 2 and Figure 3A). The $K_F$ values were calculated as 2.02, 3.21, and 7.37, while the $1/n$ values were 2.18, 2.45, and 2.11 for FeB, $FeCl_3B$, and Zr−$FeCl_3B$, respectively (Table 2). The higher $K_F$ value indicates higher $As^V$ adsorption capacity by Zr−$FeCl_3B$, where $1/n$ value describes that the $As^V$ adsorption process could be favorable.[78,79] The strong concentration gradient between $AsO_4^{3-}$ and the BC surface in the solution phase contributed to more $As^V$ adsorption.[78] Thus, $AsO_4^{3-}$ anions migrated to the heterogeneous surfaces of BCs (Figure 3B).


https://doi.org/10.1021/acsomega.1c04129
ACS Omega 2022, 7, 101−117

Table 2. Adsorption Isotherm Models and Best-Fit Parameters for $As^V$ Adsorption Data

| BC | $q_{exp}$ (mg/g) | Langmuir model parameters | | | | | Freundlich model parameters | | | | Temkin model parameters | | | Dubinin-Radushkevich model parameters | | | | |
|---|---|---|---|---|---|---|---|---|---|---|---|---|---|---|---|---|---|---|
| | | $q_{cal}$ (mg/g) | $q_m$ (mg/g) | $K_L$ (L/mg) | $R_L$ | $R^2$ | $q_{cal}$ (mg/g) | $K_F$ (g/mg/h) | $1/n$ | $R^2$ | $b$ (J/mol) | $A$ (L/g) | $R^2$ | $q_m$ (mg/g) | $E$ (kJ/mol) | $\beta$ | $R^2$ | pH |
| FeB | 21.97 | 21.70 | 27.4 | 0.02 | 0.13–0.9 | 0.98 | 24.21 | 2.02 | 2.18 | 0.98 | 5.37 | 0.26 | 0.96 | 69.84 | 9.6 | $5.3 \times 10^{-3}$ | 0.99 | 5 |
| $FeCl_3B$ | 26.28 | 25.45 | 29.77 | 0.03 | 0.09–0.86 | 0.99 | 29.13 | 3.21 | 2.45 | 0.98 | 5.84 | 0.41 | 0.99 | 71.74 | 10 | $4.6 \times 10^{-3}$ | 0.99 | 5 |
| Zr−$FeCl_3B$ | 54.39 | 53.62 | 67.28 | 0.05 | 0.05–0.77 | 0.99 | 62.74 | 7.37 | 2.11 | 0.98 | 12.81 | 0.76 | 0.97 | 223 | 9.9 | $4.8 \times 10^{-3}$ | 0.99 | 6 |

Meanwhile, the $R^2$ values of the Temkin modeled data for FeB, $FeCl_3B$, and Zr−$FeCl_3B$ were 0.96, 0.99, and 0.97, respectively (Table 2). This model (Temkin) describes the heterogeneous BC surface structure with adsorption sites that have a range of binding energies during $As^V$ adsorption (Figure 3C).[80]

The high $R^2$ (0.99) values indicated that the best isotherm fit was with the D-R model (Figure 3D). The higher theoretical $As^V$ adsorption of BCs could be ascribed to the greater microporosity and reduced pore diameter. This result also agreed with the greater specific surface area (SSA) of the BCs.

**2.2. Characterization of BC.** The pH values of FeB, $FeCl_3B$, and Zr−$FeCl_3B$ were 5.41, 5.88, and 5.64 in $H_2O$ and 5.28, 5.45, and 5.17 in $CaCl_2$, respectively, which indicated that modified BCs showed acidic characteristics, whereas raw BSBC (pH = 7.12) showed slightly basic characteristics(Table S2). The pore volume of BSBC, FeB, $FeCl_3B$, and Zr−$FeCl_3B$ was 0.006, 0.007, 0.017, and 0.019 $cm^3/g$; however, the pore size was 6.51, 5.75, 4.80, and 3.92 nm for BSBC, FeB, $FeCl_3B$, and Zr−$FeCl_3B$, respectively. The $pH_{PZC}$ also increased from 3.6 to 4.7, 4.9, and 6.3 when compared from BSBC to FeB, $FeCl_3B$, and Zr−$FeCl_3B$. The Fe content in raw BSBC was 100.69 mg/g, whereas after modification, the Fe content was increased to 176.2, 228.2, and 238.8 mg/g for FeB, $FeCl_3B$, and Zr−$FeCl_3B$, respectively. The physico-chemical characterization and elemental composition of all Fe-coated BCs are presented in Tables S2 and S3. The SSA of Fe-modified BCs, specifically FeB, $FeCl_3B$, and Zr−$FeCl_3B$, increased to 6.6, 24.02, and 25.51 $m^2/g$, respectively (Table S2), compared to the pristine BC (4.64 $m^2/g$) reported earlier.[46] Thus, increasing trends of SSA in BCs (FeB < $FeCl_3B$ < Zr−$FeCl_3B$) affected the pore size and pore volume on the coated BC surface.[81] However, surface area increases with smaller particle sizes, and this explains the higher adsorption at lower particle size.[81] The average particle size for FeB, $FeCl_3B$, and Zr−$FeCl_3B$ was determined to be 909, 249, and 235 nm, respectively. Also, SSA correlated with an increased pore volume (Table S2).[82]

The Zr particles precipitated on the BC surface, which resulted in a rough and heterogeneous surface during synthesis of the Zr−$FeCl_3B$ composite (Figure 4Ci). After reacting with As, the particle size of BCs became finer, and the morphologies of FeB, $FeCl_3B$, and Zr−$FeCl_3B$ were transformed into nonregular shaped aggregates and/or rough surfaces with elongated shards [Figure 4A(ii),B(ii),C(ii)].

The energy-dispersive X-ray spectroscopy (EDS) spectra shows evidence for the presence of sorbed As including Fe in FeB and $FeCl_3B$ (Figure 4A(iii),B(iii)). Similarly, As-spectra along with both Fe and Zr peak were confirmed in Zr−$FeCl_3B$ by EDS analysis (Figure 4Ciii). The amount of sorbed As was estimated to be 1.0 wt % (0.24 atomic %), 3.65 wt % (0.87 atomic %), and 3.89 wt % (1.93 atomic %), by FeB, $FeCl_3B$, and Zr−$FeCl_3B$, respectively (Table S4). The amount of Fe was also determined to be 24.78 wt % (7.86 atomic %), 15.32 wt % (4.91 atomic %), and 46.24 wt % (30.69 atomic %) by As-loaded FeB, $FeCl_3B$, and Zr−$FeCl_3B$, respectively (Table S4). Additionally, Zr particles were determined to be 16.84 wt % (6.84 at. %) in the As-loaded Zr−$FeCl_3B$ composite (Table S4). Results suggested that a large amount of As was adsorbed by the Zr−$FeCl_3B$ composite, which may have been due to the combined effect of Fe and Zr. This could be due to the higher SSA from the Zr−Fe loadings on the surface of BC and increased positive surface charge (zeta potential) produced


https://doi.org/10.1021/acsomega.1c04129
ACS Omega 2022, 7, 101−117

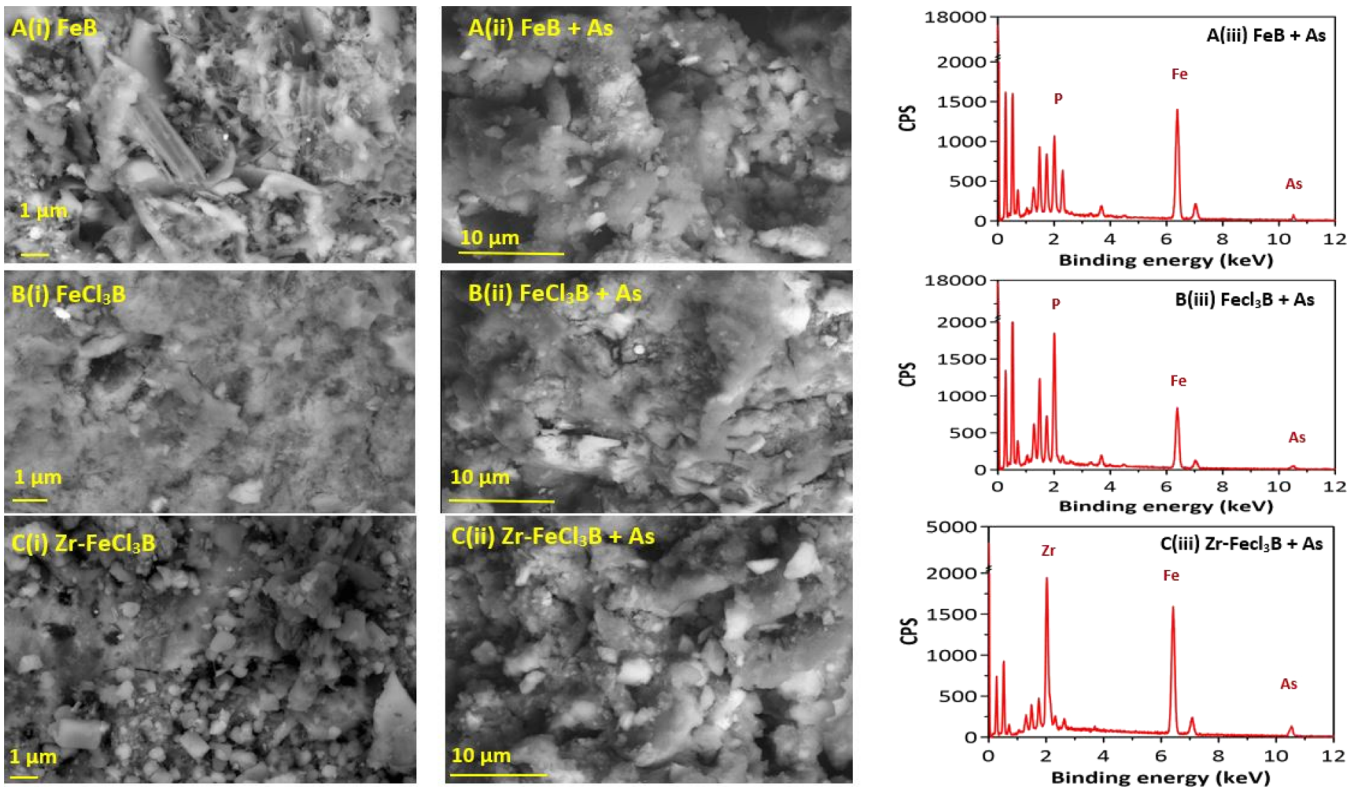


**Figure 4.** SEM micrographs of FeB, $FeCl_3$−B, and Zr−$FeCl_3$B, before A(i)−C(i) and after A(ii)−C(ii) As-adsorption; A(iii)−C(iii) represents SEM−EDS of the corresponding As-loaded BCs.

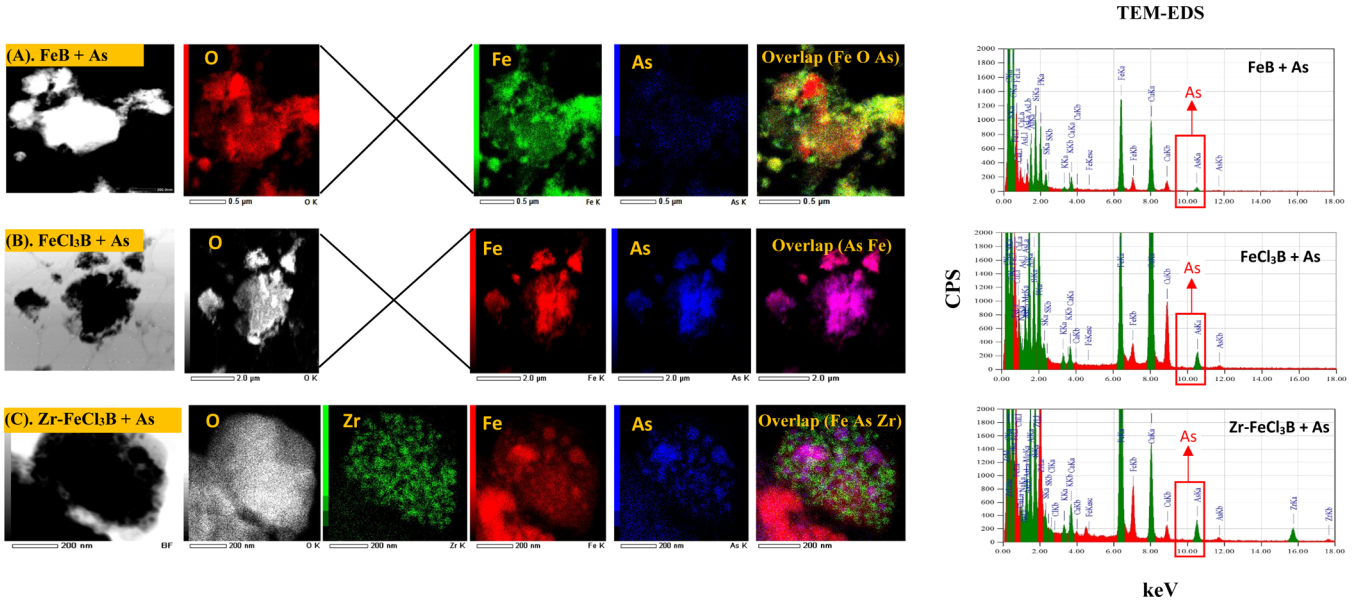


**Figure 5.** TEM elemental distribution of the As-loaded FeB (A), As-loaded $FeCl_3$B (B), and As-loaded Zr−$FeCl_3$B (C) and TEM−EDS of their respective As-loaded BCs (right side).

compared to unmodified BC and high Fe content in the Zr−$FeCl_3$B composite.

The transmission electron microscopy (TEM) elemental mapping and EDS of As-adsorbed FeB, $FeCl_3$B, and Zr−$FeCl_3$B are depicted in Figure 5. Similar to scanning electron microscopy (SEM), the HTEM images described the presence of As and other major elements like Fe and O existing on the FeB, $FeCl_3$B, and Zr−$FeCl_3$B BC surfaces (Figure 5A−C). Meanwhile, the presence of Zr particles was observed in As-loaded Zr−$FeCl_3$B composites (Figure 5C). The Zr (K-line) (mass 2.93%) was located heterogeneously on the Zr−$FeCl_3$B surface and confirmed by the TEM−EDS spectrum at 15.74 keV. The presence of As (K-line) was confirmed by TEM−EDS, while the amount of the As was determined masswise to be 0.99% As, 1.04% As, and 1.24% As in FeB, $FeCl_3$B, and Zr−$FeCl_3$B, respectively, after adsorption with As at 10.53 keV (right-hand corner of Figure 5A−C). This finding agrees with the SEM results.



https://doi.org/10.1021/acsomega.1c04129
ACS Omega 2022, 7, 101−117

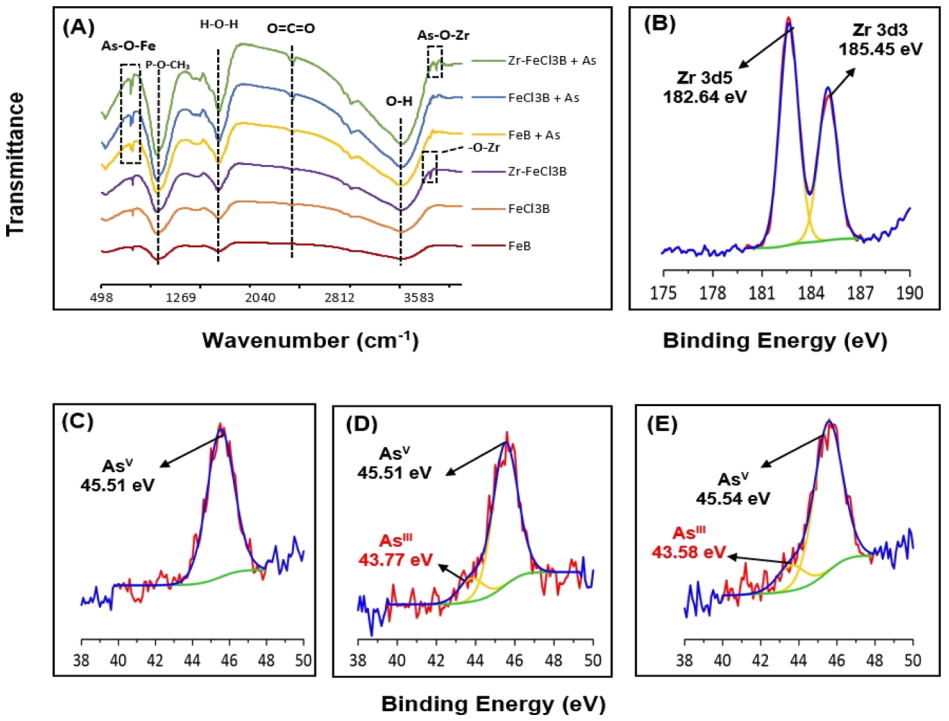


**Figure 6.** FTIR spectra of BCs before and after As-reaction (A), XPS spectra of Zr in Zr−$FeCl_3B$ (B), XPS spectra of As in As-loaded FeB (C), $FeCl_3B$ (D), and Zr−$FeCl_3B$ (E).

Before $As^V$ adsorption, the Fourier transform infrared (FTIR) spectra showed similar peaks for all BCs except for the formation of a new peak at 3695 $cm^{-1}$, which may explain the Zr−O and Zr−OH−Zr vibrations,[83,84] and confirmed the successful coating of Zr along with Fe (peak at 802 $cm^{-1}$) in Zr−$FeCl_3B$ (Figures 6A and S2A). The FTIR spectra also revealed broad band peaks at around 3400−3450 and 1620−1650 $cm^{-1}$ for all BCs. The peak close to 2300−2400 $cm^{-1}$ assigned to the presence of atmospheric $CO_2$.[85] These represent stretching and vibration peaks of −O−H and H−O−H, respectively, further indicating the bending and deformation of water molecules.[66]

After $As^V$ adsorption, a new second peak at 782 $cm^{-1}$ was observed close to 802 $cm^{-1}$ after reacting with As (Figure S2A), which is attributed to symmetric vibrations between As−O− and As−O−Fe complexation, which was supported by past studies.[66,86] Another new peak was observed at 3748 $cm^{-1}$ in the As-reacted Zr−$FeCl_3B$ BC (Figure S2B), and this may be caused by the formation of an inner As−O−Zr complex. The spectra at 3730 and 3745 $cm^{-1}$ reported the presence of a bi-bridged hydroxyl group on Zr−$O_2$.[84,87,88] Therefore, it can be assumed that the peak 3695 $cm^{-1}$ (observed in Zr−$FeCl_3B$) (Figure S2B) could be shifted to 3748 $cm^{-1}$ (close to 3745 $cm^{-1}$) after the interaction between As and Zr−O groups.

The observed peaks at 22.97, 24.28, 31.16, 36.95, and 53.38° in the XRD pattern represented different types of trigonal (hexagonal axes) quartz (silica) and graphite, in Fe-coated or Zr−Fe coated BCs (Figure S3A). No confirmed peaks corresponding to Zr and/or Fe coatings in the XRD spectrum of the modified BCs were observed (Figure S3A), which suggested that Fe- and/or Zr−Fe-associated BCs existed predominantly in the amorphous phases. The formation of amorphous Fe-oxide/hydroxides on BC and Fe-granular activated carbon composites are documented in the literature.[89−91] No As-related minerals were detected when employing XRD analysis in this study (Figure S3B).

XPS analysis of the survey profile revealed enriched amounts of C, O, N, and Fe on the BCs' surface (Figure S3). The Zr peak was observed in two binding energies at approximately 182.64 eV (Zr $3d_{5/2}$) and 185.45 eV (Zr $3d_{3/2}$), which represented Zr-oxide[92,93] on the Zr−$FeCl_3B$ surface (Figure 6B). XPS survey analysis also confirmed the As 3d spectrum on the BC surface (Figure S4). Ren et al. (2011)[66] and Ding et al. (2000)[94] reported that the values of As 3d core level of $As^V$ may move to between 45.31 and 45.6 eV during the adsorption of As. In this study, the XPS spectrum at bonding energies of 45.51, 45.51, and 45.54 eV correspond to $As^V$ in the As 3d region for FeB, $FeCl_3B$, and Zr−$FeCl_3B$, respectively[95] (Figure 6C−E).

**2.3. Influence of Interfering Ions.** The anions $Cl^-$, $NO_3^-$, $CO_3^{2-}$, $SO_4^{2-}$, and $PO_4^{3-}$ are commonly present in natural waters, which can potentially interfere with $As^V$ adsorption. Chloride and $NO_3^-$ had no effect on $As^V$ adsorption, which may be due to their negligible affinities for the BC surface. The $As^V$ removal efficiency was reduced by 15, 14, and 7% in FeB, $FeCl_3B$, and Zr−$FeCl_3B$ in the presence of $SO_4^{2-}$, which may have little affinities toward the BC surface. The $Cl^-$ and $NO_3^-$ anions mainly form outer-sphere complexes with Fe-oxy compounds[96] and thus inhibitory $As^V$ adsorption to a minor extent on Fe-modified BC surfaces.

The $As^V$ removal ability declined by 49, 45, and 35% in the presence of $CO_3^{2-}$. Schmidt et al. (2020)[97] and Mendez and Hiemstra (2018)[98] reported that $SO_4^{2-}$ and $CO_3^{2-}$ can form inner-sphere complexes with Fe-oxide surfaces and thus affected $As^V$ adsorption by Fe-modified BC. The $PO_4^{3-}$ ion was the greatest competitive anion, and it significantly inhibited $As^V$ adsorption by 88, 85, and 75% for FeB, $FeCl_3B$, and Zr−$FeCl_3B$, respectively, compared to $NO_3^-$ (Figure 7A−C). The adsorption capacity of $As^V$ decreased


https://doi.org/10.1021/acsomega.1c04129
ACS Omega 2022, 7, 101−117

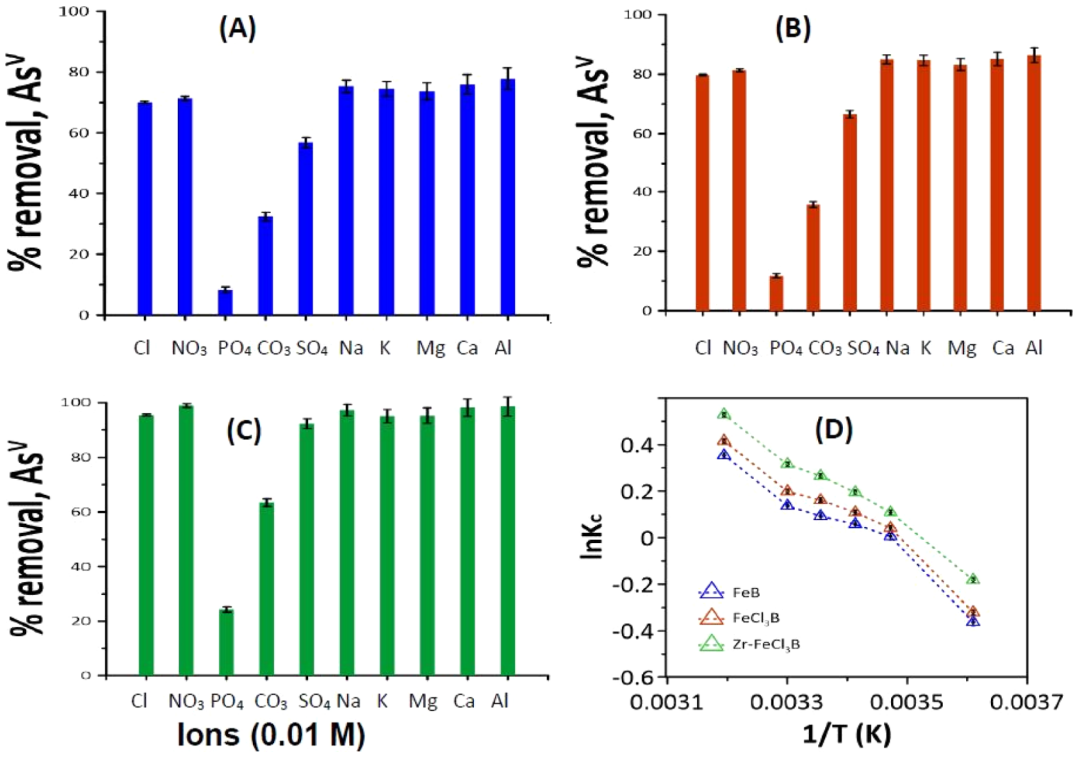


**Figure 7.** Effect of interfering ions (A) FeB, (B) $FeCl_3B$, and (C) Zr−$FeCl_3B$ (the initial $As^V$ concentration was 20 mg/L, and BC density was 2 g/L at 22 ± 0.5 °C) and (D) temperature of $As^V$ adsorption on BCs (the initial $As^V$ concentration was 10 mg/L).

**Table 3. Thermodynamic Parameters for the Adsorption of $As^V$ on BCs**

| | $\Delta G$ (kJ/mol) | | | | | | | | |
|---|---|---|---|---|---|---|---|---|---|
| BC | 277 K | 288 K | 293 K | 298 K | 303 K | 313 K | $\Delta H$ (J/mol) | $\Delta S$ (J/mol.K) | pH |
| FeB | −12.47 | −12.96 | −13.19 | −13.42 | −13.64 | −14.09 | 13.17 | 45.06 | 5 |
| $FeCl_3B$ | −13.1 | −13.62 | −13.86 | −14.1 | −14.33 | −14.81 | 13.72 | 47.35 | 5 |
| Zr−$FeCl_3B$ | −13.23 | −13.76 | −14.0 | −14.24 | −14.48 | −14.95 | 13.6 | 47.82 | 6 |

from 7.62 to 0.91 mg/g (at solution pH 5), 7.98 to 1.19 mg/g (at solution pH 5), and 9.41 to 2.35 mg/g (at solution pH 6) in the presence of $PO_4^{3-}$ with FeB, $FeCl_3B$, and Zr−$FeCl_3B$, respectively, using 2 g/L BC doses rate and at 22 ± 0.5 °C. This substantial inhibitory effect could be due to the similar molecular structures of $PO_4^{3-}$ and $AsO_4^{3-}$, which creates a strong competition for binding sites of BCs.[99] Moreover, $PO_4^{3-}$ is able to compete for the same adsorption sites of $AsO_4^{3-}$ forming inner-sphere complexes in the presence of Fe-oxy-hydroxides.[100,101]

The influence of common cations such as $K^+$, $Na^+$, $Mg^{2+}$, $Ca^{2+}$, and $Al^{3+}$ on $As^V$ adsorption toward FeB, $FeCl_3B$, and Zr−$FeCl_3B$ was assessed. No noteworthy effect was observed on $As^V$ adsorption by FeB, $FeCl_3B$, and Zr−$FeCl_3B$ in the presence of these cations (Figure 7A−C).

**2.4. Effect of Temperature.** The calculated thermodynamic parameters, including $\Delta G$, $\Delta H$, and $\Delta S$, are listed in Table 3. The $As^V$ removal efficiency rose as the temperature increased from 4 to 40 °C (277−313 K) (Figure 7D). The negative ΔG values indicate that the adsorption process is spontaneous at 4−40 °C (Tables 3 and S5).[35] The mobility of $As^V$ ions increases with increasing solution temperature; therefore, elevated $As^V$ removal capacity was achieved by the BC composites.[102] The obtained $\Delta H$ values were positive, which demonstrated that the $As^V$ adsorption process was endothermic for all BCs.[76]

The positive $\Delta S$ value means that the adsorption process was favorable but had increased randomness of $As^V$, leading to a more disordered state on the BC/solution interface.[35] In addition to this, ion solvation could play a role in increasing entropy ($\Delta S$).[103,104] In this study, the higher positive change in enthalpy and increase in entropy collectively contributed to the strong spontaneous adsorption of $As^V$ by all Fe-coated BCs.

**2.5. Reusability of BCs.** After successful $As^V$ adsorption, the As-loaded FeB, $FeCl_3B$, and Zr−$FeCl_3B$ were subjected to regeneration tests in order to determine reusability and stability of BCs. The experiment consisted of up to six adsorption−desorption cycles to examine repetitive usage of BCs under optimum conditions. Results showed that the adsorption capacities of all BCs slightly reduced after six adsorption−desorption cycles (Figure 8). Very low desorption capacity was observed with MQ water for FeB (8.38−4.98%), $FeCl_3B$ (7.88−5.11%), and Zr−$FeCl_3B$ (5.77−4.72%), respectively (Figure 8A(i)−C(i)). The percentages of desorbed As ranged from 75.14 to 55.14, 78.11 to 73.17, and 80.43 to 74.87 up to six trials by FeB, $FeCl_3B$, and Zr−$FeCl_3$ BCs, respectively, when using $(NH_4)_2SO_4$ (Figure 8 Aii−Cii). The desorption efficiencies of FeB, $FeCl_3B$, and Zr−$FeCl_3B$ decreased from 95.7 to 89.75, 96.96 to 91.4, and 99.1 to 95.73%, respectively, from the first to the sixth trial using NaOH (Figure 8A(iv)−C(iv)). Results showed that the desorbing solution of $HNO_3$ followed almost the same pattern


https://doi.org/10.1021/acsomega.1c04129
ACS Omega 2022, 7, 101−117

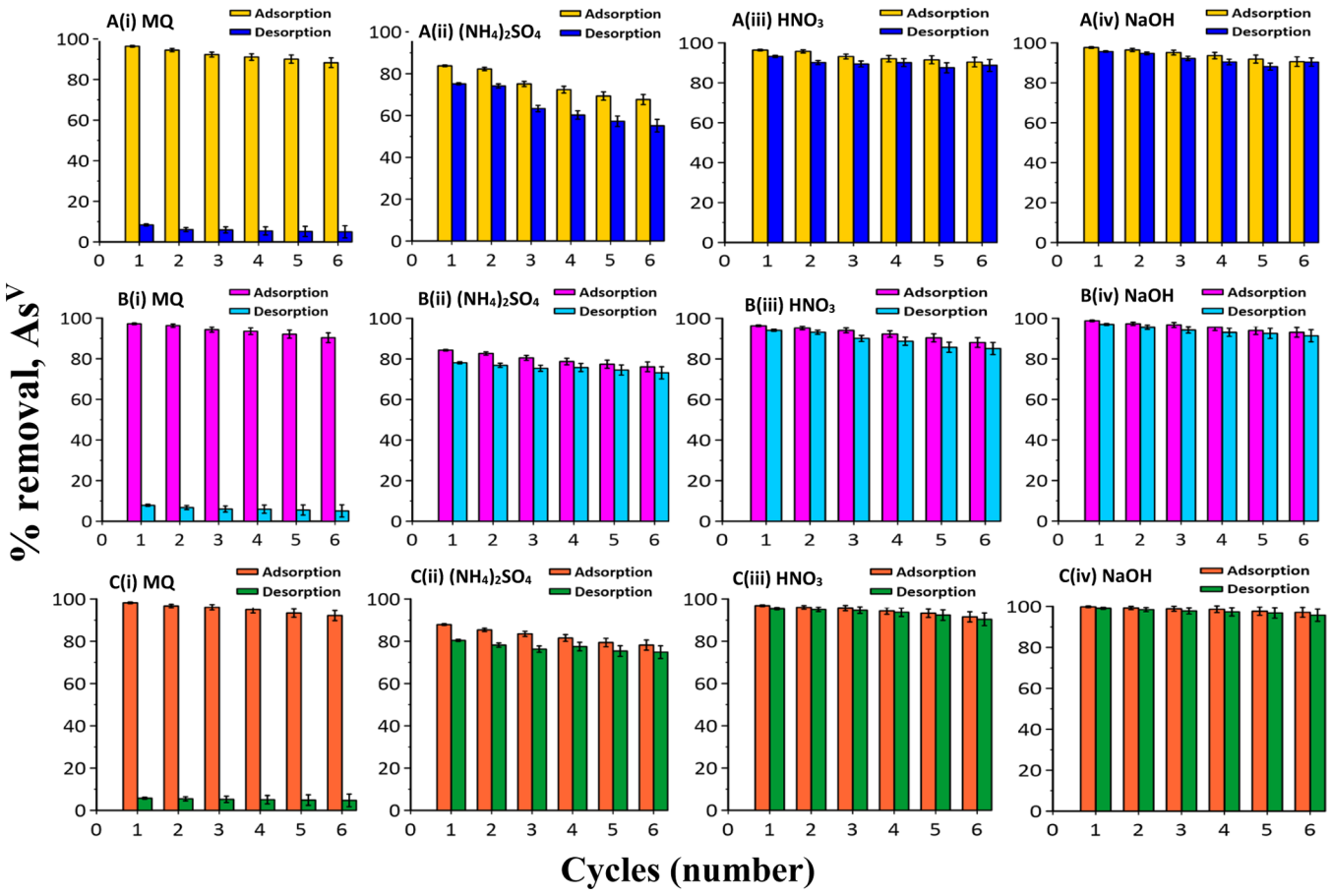


**Figure 8.** Adsorption−desorption of As-loaded (A) FeB, (B) $FeCl_3B$, and (C) Zr−$FeCl_3B$ (BC density was 2 g/L under optimum conditions).

as NaOH; however, NaOH was a more efficient desorbing agent than $HNO_3$ for all Fe-coated BCs. The leached Fe ions from FeB, $FeCl_3B$, and Zr−$FeCl_3B$ were determined to be 0.63, 0.72, and 0.35 mg/L after the first regeneration cycle, while the concentration of Fe was 0.74, 0.86, and 0.44 mg/L after the six cycles at pH 5. Zr leached from Zr−$FeCl_3B$ was 0.08 and 0.13 mg/L after the first and sixth adsorption−desorption cycle, respectively, at pH 5.

The sequence for the examined materials' reusability was Zr−$FeCl_3B$ > $FeCl_3B$ > FeB, respectively. Results suggested that all Fe-modified BC composites—FeB, $FeCl_3B$, and Zr−$FeCl_3B$—were effectively recycled and can be employed in repeated $As^V$ adsorption batches at least six times with minimum loss in their adsorption capacities[35] using NaOH as the preferred desorption agent.

**2.6. Role of Fe and Zr in $As^V$ Adsorption.** Oxides of Fe and Zr generally have strong binding affinities toward $As^V$. Arsenate could attract both Fe−OH and Zr−OH surface sites on the BC through the possible formation of $FeAsO_4$ and $Zr_3(AsO_4)_4$ surface precipitates.[65] The Zr−OH sites prefer to bind with $As^V$ compared to Fe−OH sites. The reason for this may be due to the low solubility product constant of $Zr_3(AsO_4)_4$ compared to $FeAsO_4$ ($K_{sp}$ = 1.47 × $10^{-9}$). Another reason could be the predominant formation of the $Zr_3(AsO_4)_4$ phase rather than $FeAsO_4$ phases, when free $AsO_4^{3-}$ concentrations were insufficient compared to additional Zr−OH or dissolved $Zr^{4+}$ onto the BC surface.[65] Therefore, Zr−OH- or Zr-coated surface sites are much stronger than Fe−OH sites, which was also suggested by previous studies.[65] The maximum $As^V$ sorption capacities of pristine and Zr-modified biosolid BC (Zr-BSBC) were reported to be 15.2 and 33.1 mg/g, respectively.[46] In the current study, binary metal Zr−Fe-coated BCs (67.28 mg/g) have shown improved $As^V$ adsorption efficiency compared to single Fe coatings only (27.4 and 29.77 mg/g). This is attributed to the co-presence of Zr and Fe, which increased the SSA and bound more strongly with $As^V$. However, the surface area of Zr−$FeCl_3B$ (25.51 $m^2$/g) was almost similar to FeB (24.02 $m^2$/g). Previous studies showed that even single metal Zr-coated BC (75.9 $m^2$/g) showed much higher surface area compared to binary Zr−Fe-chip-coated BC (27.9 $m^2$/g).[46] This could be due to the geometric position (hindering effect) of the Zr and Fe atoms on the BC surface. Therefore, Zr−OH had the most active sites responding to $As^V$, and thus, $As^V$ tends to bind more favorably to Zr−O moieties.[65] Despite the inability to detect Zr or As crystallinity by XRD, the SEM−EDS and TEM−EDS also support this outcome.

The presence of Fe was 6.4% Fe, 8.60% Fe, and 19.90% Fe, whereas the amounts of O in mass were 8.35% O, 12.9% O, and 19.95% O, respectively, in Fe-coated FeB, $FeCl_3B$, and Zr−$FeCl_3B$ BC composites by TEM−EDS analysis. The ratios of O/Fe were determined to be 1.3, 1.5 and 1.0, while the ratios of O/As were 8.43, 12.4, and 16.08, respectively, in FeB, $FeCl_3B$, and Zr−$FeCl_3B$. However, the ratio of O/Zr was calculated to be 7.02 in the Zr−$FeCl_3B$ composite. Results revealed that at higher O/As, there was more As sorbed by BCs. The ratio of O/Fe in Zr−$FeCl_3B$ was comparatively low compared to FeB and $FeCl_3B$ BCs. This is because the


https://doi.org/10.1021/acsomega.1c04129
ACS Omega 2022, 7, 101−117

additional presence of Zr with Fe in the Zr−$FeCl_3B$ composite reduced the O/Fe ratio due to the high affinity toward Zr and O rather than Fe and O (electronegativity of O, Zr, and Fe are 3.44, 1.33, and 1.83). These results clearly indicated that the role of O/Fe and/or O/Zr for enhancing the removal of As by Fe- and Fe−Zr-coated BC composites compared favorably to pristine BSBC (Table 4). The XPS documented a similar result.

**Table 4. Comparison of Removal Capacity of $As^V$ Using Various Pristine and Modified BCs**

| BCs | $As^V$ adsorption capacity, (mg/g) | References |
|---|---|---|
| BSBC | 15.2 | 46 |
| almond shell | 3.6 | 106 |
| ZnO-modified coffee husk | 1.54 | 107 |
| ZnO-modified corncob | 25.9 | 107 |
| corncob | 13.06 | 107 |
| rice straw | 11.2 | 108 |
| | 0.55 | 109 |
| red mud-modified rice straw | 5.92 | |
| $Fe^{2+}$- and $Fe^{3+}$-modified rice straw | 26.9 | 108 |
| $ZnCl_2$-modified crayfish shell | 17.2 | 110 |
| yak dung | 1.05 | 111 |
| $FeCl_2{\cdot}4H_2O$ + NaClO-modified yak dung | 2.93 | |
| perilla leaf | 2.95 | 14 |
| Japanese oak wood | 3.89 | 37 |
| Fe-impregnated corn straw | 6.80 | 112 |
| $FeCl_3$-modified *Cassia fistula* (golden shower) | 1.07 | 113 |
| nZVI-modified red oak | 15.66 | 114 |
| nZVI-modified switchgrass | 6.48 | |
| chestnut shell | 17.5 | 41 |
| magnetic gelatin-chestnut shell | 45.8 | 41 |
| paper mill sludge | 23.1 | 115 |
| Ni/Fe-modified pinewood | 6.52 | 44 |
| rice husk | 0.42 | 116 |
| | 2.59 | 117 |
| | 7.1 | 118 |
| bismuth oxide-modified Wheat straw | 16.21 | 119 |
| empty fruit bunch | 18.9 | 118 |
| $Fe^{2+}$- $Fe^{3+}$-modified Water hyacinth | 7.41 | 120 |
| Zr-BSBC | 33.1 | 46 |
| Fe-chip-coated BSBC | 27.4 | this study |
| Fe-salt-coated BSBC | 29.77 | this study |
| Zr−Fe-salt-coated BSBC | 67.28 | this study |

### 2.7. Redox Transformation of $As^V$ to $As^{III}$ on BCs.

Analysis of high-resolution XPS spectra showed a single peak of As 3d at the binding energies of 45.51 eV in FeB BC surface, after reacting with $As^V$. The peaks appearing at 45.51 eV confirmed the presence of $As^V$ on FeB and $FeCl_3B$ BC (Figure 6C,D). Interestingly, two peaks of the As 3d region appeared at 45.51 eV and 43.77 eV in $FeCl_3B$ and 45.54 eV and 43.58 eV in Zr−$FeCl_3B$ BC solid surface after adsorption with $As^V$, which confirmed the co-existence of both $As^V$ (45.51 and 45.54 eV) and $As^{III}$ (second small peak at 43.77 and 43.58 eV) on BC surfaces (Figure 6D,E and Table S6).[41,105] Results suggest that redox transformation of $As^V$ (86.4 and 84.9%) to $As^{III}$ (13.6 and 15.1%) occurred onto $FeCl_3B$ and Zr−$FeCl_3B$ BC surfaces during adsorption despite the oxic reaction environment.

The XPS spectra revealed that the second peak produced at 185.45 eV in the Zr $3d_{3/2}$ region corresponds to the Zr−$O_2$[93,121] (Figure 6B). Lewis acid−base definition classified Zr to be more basic than Fe species ($Fe^{2+}$ or $Fe^{3+}$) which also enables Zr to function as a reductant.

It is previously reported that $Fe^{III}$ could influence surface reduction from $As^V$ to $As^{III}$;[122] therefore, the presence of $Fe^{III}$, reduction of $As^V$ occurred in $FeCl_3B$ and Zr−$FeCl_3B$ BC surfaces. However, further research should be explored to understand the probable mechanism and the role of Fe and Zr behind this reduction. As the toxicity of $As^{III}$ is greater than $As^V$ and it is extremely difficult to remove $As^{III}$, this finding of As transformation has practical implications and needs more research to determine the extent of reduction from $As^V$ to $As^{III}$.

According to the literature, it can be assumed that a passive layer was formed on the Fe-based adsorbent surface during adsorption of $Cr^{VI}$, which could prevent the reduction of $Cr^{VI}$ to $Cr^{III}$.[123,124] Therefore, further studies should include the modification of BC materials to control the redox transformation of As during the adsorption process.

The XPS peaks for the Fe 2p shell in the Fe $2p_{3/2}$ (the more intensive of two peaks Fe 2p) and Fe $2p_{1/2}$ subshells (without extra excitation) and satellite structure is observed for different Fe compounds. This is due to the multiple splitting and electron shake up. The three Fe $2p_3$ spectra at binding energies of 711.76, 715.76, and 720.06 eV (Figure 9) were detected on the surface of the FeB, $FeCl_3B$, and Zr−$FeCl_3B$ BCs, respectively, before reaction with As (Table S6). The spectra at binding energies 711.76, 711.41, and 711.19 eV indicated the presence of $Fe^{3+}$ (Figure 9) as Fe$2p_{3/2}$ ($FeCl_3$ or $Fe_2O_3$),[121,125] whereas the spectra at 715.76, 714.89, and 714.46 eV represent the multiplet spectra of $Fe^{3+}$ as Fe $2p_{3/2}$ (Figure 9) ($FeCl_3$ or $Fe_2O_3$) for FeB, $FeCl_3B$, and Zr−$FeCl_3B$, BCs.[125−127] Another XPS satellite structure of $Fe^{3+}$ as Fe $2p_{3/2}$ (Figure 9) was detected at 720.06, 719.42, and 719.23 eV, respectively, for FeB, $FeCl_3B$, and Zr−$FeCl_3B$ BCs, which demonstrated aspects of overlapping undissolved oxidized $Fe^{3+}$ ($Fe_2O_3$) and metallic Fe.[125,126,128] Added to these, three Fe $2p_{1/2}$ (Fe $2p_{1/2}$A, Fe $2p_{1/2}$B, and Fe$2p_{1/2}$C) spectral peaks were observed at the 725−733 eV region, which describes the precipitation of combined $Fe^{2+}$ and $Fe^{3+}$ species on the BC surface during synthesis of Fe coatings.[126]

Similar XPS spectra of Fe $2p_{3/2}$ and Fe $2p_{1/2}$ peaks were detected in As-reacted BCs (Figure 9A(ii)−C(ii)). However, the peak intensity and BE positions of Fe $2p_{3/2}$, Fe $2p_{1/2}$, and satellite structures were reduced. The atomic percentages of Fe $2p_{3/2}$A, Fe $2p_{3/2}$B, and Fe $2p_{3/2}$C were reduced to 3−1.8, 1.02−0.52, and 0.86−0.42% for FeB, 4.02−2.48, 1.51−0.78, and 1.23−0.53 for $FeCl_3B$, and 3.44−1.8, 1.32−0.59, and 0.98−0.4 for Zr−$FeCl_3B$, respectively, after reacting with As (Table S6). Therefore, a minor shift in the Fe 2p and Zr 3d species occurred while reacting with As. In addition, the O1s XPS spectra divided into three forms with binding energy corresponding to 530.23−530.27 eV (lattice $O^{2-}$), 531.52−531.55 eV (−OH), and 532.86−532.86 eV (C═O)[125] in FeB and Zr−$FeCl_3B$, respectively, after reacting with As (Figure S5). However, two O 1s spectra at 531.57 eV (−OH) and 532.88 eV (C═O) were found in As-reacted FeB (Figure S5). All these results confirm the strong bonding of As with Zr and Fe species via the formation of inner sphere As−O−Fe in FeB and $FeCl_3B$ BCs;[129] and As−O−Fe and As−O−Zr complexation was evident in the Zr−$FeCl_3B$ BC. Previous studies from


https://doi.org/10.1021/acsomega.1c04129
ACS Omega 2022, 7, 101−117

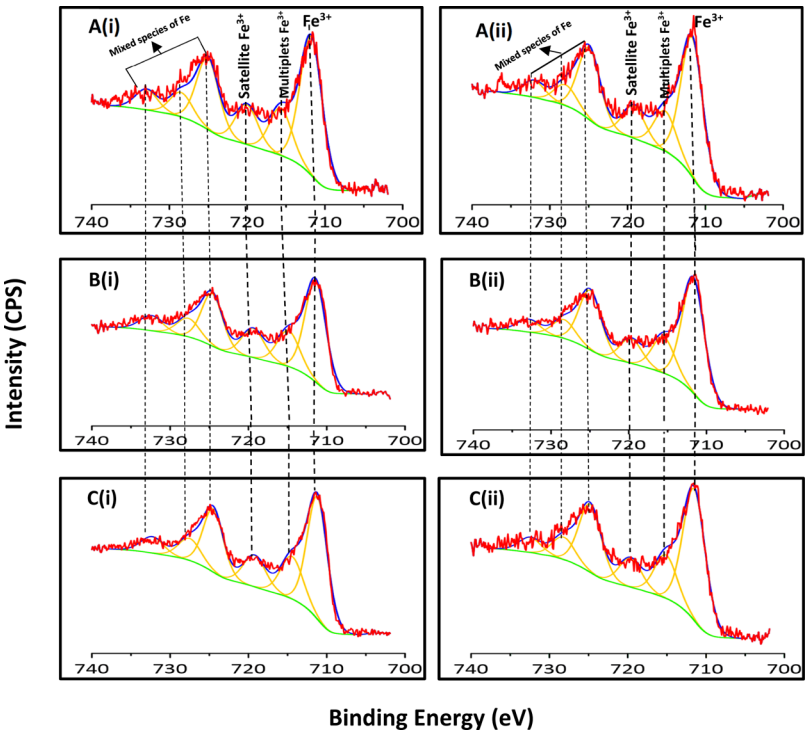


**Figure 9.** High-resolution XPS spectrum of Fe 2p before A(i)−C(i) and after A(ii)−C(ii) reaction with As by FeB, $FeCl_3B$, and Zr−$FeCl_3B$, respectively.

Peng et al. (2022)[121] and Fang et al. (2021)[130] also supported this.

## 3. CONCLUSIONS

The study demonstrated that Fe and combined Zr−Fe can be utilized to modify BCs to maximize the adsorption capacity of $As^V$. The adsorption capacity of Zr−Fe-modified BC was increased by 4.43, 2.45, and 2.3 folds when compared to the BSBC, Fe-BSBC, and Zr-BSBC, respectively (Table 4). The adsorption of $As^V$ is pH dependent, and the maximum adsorption was obtained under acidic conditions. The Langmuir maximum $As^V$ removal efficiencies were found to be 27.4, 29.77, and 67.28 mg/g by FeB (at pH 5), $FeCl_3B$ (at pH 5), and Zr−$FeCl_3B$ (at pH 6), respectively. Zeta potential and $pH_{PZC}$ value are increased by bimetal Zr−Fe coatings (Tables S1 and S2). The presence of Zr resulted in the greatest $As^V$ removal from solution. This may be due to the enhanced SSA with bimetal Zr−Fe coatings on the BC surface, and an increase in the positive surface charge produced compared to pristine and single Fe-modified BC. Among the anions tested, $PO_4^{3-}$ greatly competed in the adsorption process that reduced the $As^V$ removal of 88, 85, and 75% with FeB, $FeCl_3B$, and Zr−$FeCl_3B$, respectively, due to the strong affinity of $As^V$ active sites. Thermodynamic investigations demonstrated that the adsorption process is favored, and the $As^V$ removal capacity of all Fe-coated BCs increased when the temperature increases from 277 to 313 K. Fe-modified BC is promising for $As^V$ removal from aqueous solution as the Fe-modified BC composites are economical and efficient in removing $As^V$ (>85%) from contaminated waters in repeated six adsorption−desorption cycles. The XPS spectra confirmed the transformation of $As^V$ (86.4 and 84.9%) to the more toxic species $As^{III}$ (13.6 and 15.1%) and during adsorption with single $FeCl_3B$ and binary Zr−Fe-coated BSBC. Further research is required to confirm the redox transformations of As species and how to reduce such reduction to abate the potential toxicity of $As^{III}$ during adsorption. In addition, the possible role of shared charge in $PO_4^{3-}$, $SO_4^{2-}$, and $CO_3^{2-}$ competitive adsorption with As species needs to be explored further. This could provide useful information for practical and sustainable usage of the proposed materials.

## 4. MATERIALS AND METHODS

**4.1. Preparation of BC.** The BS biomass (BSBM) was collected from Winmalee sewage treatment plant in Winmalee, NSW, Australia. The BSBM was stored at approximately 24 °C after being oven dried at 80 °C for 24 h. Slow pyrolysis was employed for producing pristine BC from BSBM at a peak temperature of 300 °C for 30 min at a heating rate of 7 °C $min^{-1}$ as per Rahman et al. (2021c).[131] Briefly, 50 g of air-dried and ground (<1 mm, 50 mesh) biomass was employed in a ceramic crucible covered with a lid and heated in a muffle furnace under a $N_2$ atmosphere. The resulting BSBC samples were allowed to cool at room temperature inside the furnace. Afterward, the BSBC was removed from the furnace, stored in airtight plastic containers, and preserved in a desiccator for further modifications.

**4.2. Synthesis of Fe- and Zr−Fe-Modified BC.** Iron chips (Fe) and iron-salt ($FeCl_3{\cdot}6H_2O$) were separately used to synthesize Fe-BCs by employing an *in situ* precipitation method according to Rahman et al. (2021b).[85] To this end, 5.58 g Fe-chips [(Fe-chips (99.98% purity) was purchased from Sigma)] was dissolved in 100 mL of HCl (1:1) to prepare 0.1 M Fe-chips solution. Following this, 5.0 g of ground BSBC (<1 mm) was submerged into a 50 mL of Fe-chips or Fe-salt solution (0.1 M $FeCl_3{\cdot}6H_2O$) (mass ratio of Fe to BC = 1:1) adjusted at pH 6.5 by adding 0.1 M NaOH. Thus, the resulting BC suspension was aged for 12 h at room temperature. A


https://doi.org/10.1021/acsomega.1c04129
ACS Omega 2022, 7, 101−117

bimetal adsorbent-like Zr−$FeCl_3.6H_2O$ BC composite (Zr to Fe molar ratio 1:5) was synthesized following the same method, as described by Rahman et al. (2021b).[85] All synthesized BC composites were rinsed 3−4 times with MQ water to remove any impurities followed by centrifugation (5000 rpm for 15 min) and finally dried in an oven at 80 °C. The produced BCs were preserved in a desiccator after being labeled as FeB, $FeCl_3$B, and Zr−$FeCl_3$B, respectively, for further experiments.

**4.3. Adsorbent Characterization.** The point of zero charge ($pH_{PZC}$) and zeta potentials were determined using a NanoPlus HD analyzer (Micromeritics, USA). SSA, pore volume, and pore size distribution were determined by Brunauer−Emmett−Teller and Barrett−Joyner−Halenda using $N_2$ adsorption (Tristar II 3020, Micromeritics, USA). A LECO TruMac C/N/S analyzer measured the elemental composition (C, N, and S). The surface crystallinity, morphology, and functional groups were investigated with XRD (Empyrean, PANalytical), an environmental scanning electron microscope (SEM, Zeiss Sigma, Germany), a Bruker EDS detector, and FTIR (Agilent Cary 600). Furthermore, the micromorphology was determined with high-resolution TEM (HRTEM, JEM-2100F, Japan) coupled with an EDS detector (JEOL-JED-2300). The concentration of As in the BC-aqueous phase was analyzed by inductively coupled plasma optical emission spectrometry (ICP-OES, PerkinElmer Avio 200, USA). The surface oxidation state and elemental compositions of As were detected utilizing XPS (ESCA-LAB250Xi, Thermo Scientific, UK). Details of each method are described in the Supporting Information section.

**4.4. $As^V$ Adsorption Experiments Using BCs.** Kinetics studies were controlled at a ratio of 1 to 500 (BC to suspension) using 0.05 g of BC in 25 mL of solution of 50 mL centrifuge tubes containing 10 mg/L $As^V$ for 7 days followed by centrifuging at 5000 rpm for 15 m. Following this, the supernatant was filtrated utilizing 0.22 $\mu$m pore size nylon membrane filters. Adsorption isotherms were conducted using the same method as the kinetics but employing various concentrations of $As^V$ (1−250 mg/L) for a reaction period lasting 48 h. The pH versus adsorption edge experiment was carried out in the pH range 2−11 at an $As^V$ concentration of 10 mg/L. The pH of each BC suspension was controlled by adding 0.1 M $HNO_3$ and/or 0.1 M NaOH.

The adsorption capacity and removal efficiency (%) of $As^V$ onto BCs were calculated, respectively, using eqs 1 and 2.[14,46] These equations are written below as follows

$$q_e = \frac{(C_i - C_e) \times V}{W} \tag{1}$$

$$\%\text{removal As(V)} = \frac{(C_i - C_e)}{C_i} \times 100 \tag{2}$$

where $q_e$ (mg/g) represents the adsorbed amount of $As^V$ by the adsorbent, and $C_i$ and $C_e$ are the initial and equilibrium $As^V$ concentration (mg/L), respectively, while $V$ denotes the total volume (L) of the medium, and $W$ stands for the weight (g) of BC.

Different ratios of BC to solution, specifically 1:100, 1:250, 1:500, 1:1000, and 1:1500 were maintained to optimize the adsorbent dosage on $As^V$ adsorption. Competitive anions such as $Cl^-$, $NO_3^-$, $SO_4^{2-}$, $CO_3^{2-}$, and $PO_4^{3-}$ and cations such as Na, K, Mg, Ca, and Al at concentrations of 0.1 M were also investigated for $As^V$ adsorption. Various concentrations of electrolytes, these being 0.01, 0.1, 0.25, 0.5, and 1.0 M $NaNO_3$, were employed to determine the influence of ionic strength toward $As^V$ adsorption. The pH levels of BCs suspensions were maintained at 6.0 using $HNO_3$ (0.1 M) and NaOH (0.1 M), preserving BC density (2 g/L) and $As^V$ concentration (20 mg/L) at 22 ± 0.2 °C. All experiments (pH, kinetics, adsorption isotherms, and competitive ions) were conducted using 0.01 M $NaNO_3$ as the background electrolyte, and BC density was 2 g/L at temperature of 22 ± 0.5 °C. All analyses were performed in triplicate, and the average values were recorded. These includes thermodynamic studies.

All the parameters in kinetics and isotherm models are obtained through fitting the experimental raw data. The intuitive way to fit the raw data is to do a non-linear fit with the expression directly from the kinetics and isotherms equation using OriginPro software (Version 19).

**4.5. Effect of Temperature on $As^V$ Adsorption.** The thermodynamic parameters, namely, change of entropy ($\Delta S$), enthalpy ($\Delta H$), and the Gibbs free energy ($\Delta G$) are important for documenting a reaction spontaneity calculated using the linearized van 't Hoff equations as follows (eqs 3−5).[76]

$$\Delta G = -RT \ln K \tag{3}$$

$$Kc = q_e/C_e \tag{4}$$

$$\Delta G = \Delta H - T\Delta S \tag{5}$$

where $R$ is the ideal gas law constant [$8.314 \times 10^{-3}$ kJ/(mol K)], $T$ is the absolute temperature (K), and $Kc$ is the distribution coefficient, which is the ratio of the equilibrium adsorption quantity ($q_e$) to the equilibrium concentration ($C_e$) of $As^V$. The final equation can be written as

$$\ln K = \Delta S/R - \Delta H/(RT) \tag{6}$$

Based on eq 4, $\Delta H$ and $\Delta S$ parameters can be calculated from the slope and intercept, respectively, of the plot of ln $K_c$ versus $1/T$ using eq 7

$$\Delta H = -\text{slope} \times R \text{ and } \Delta S = \text{intercept} \times R \tag{7}$$

Six different temperatures including 4, 15, 20, 25, 30, and 40 °C were employed in order to investigate the influence of temperature on $As^V$ adsorption by all adsorbents maintaining isobaric and isochoric thermodynamic phases at constant pressure ($P$) and volume ($V$), respectively. The calculated thermodynamic parameters including $G$ were expressed as reaction $G$ (the change in the free energy of the reaction).

**4.6. Desorption Study and Reusability of BCs.** The $As^V$-loaded BCs were regenerated by extraction with 25 mL of MQ water, $HNO_3$ (0.1 M), NaOH (0.1 M), and ammonium sulfate [$(NH_4)_2SO_4$] (0.05 M), after washing and oven drying in six adsorption−desorption cycles separately. This was followed by continuous shaking for 24 h at 22 ± 0.5 °C. The ICP−MS determined the desorbed $As^V$, while the desorption efficiency of BCs was calculated using equation (eq 8).[46,80]

$$\%\text{ desorption, } As^V = \frac{C_{des}}{C_{ads}} \times 100 \tag{8}$$

where $C_{des}$ and $C_{ads}$ are, respectively, the desorbed amount (mg/L) of $As^V$ in the solution and adsorbed amount of $As^V$ by BCs.



https://doi.org/10.1021/acsomega.1c04129
ACS Omega 2022, 7, 101−117

Similar to the adsorption study, a 0.01 M $NaNO_3$ solution was used as the background electrolyte, and BC density was 2 g/L at 22 ± 0.5 °C. An overview of experimental conditions are tabulated in Table S7 in Supporting Information section.

## ■ ASSOCIATED CONTENT

### Supporting Information

The Supporting Information is available free of charge at https://pubs.acs.org/doi/10.1021/acsomega.1c04129.

Reagents and materials, characterization of adsorbents, adsorption kinetic models, and adsorption isotherm models (PDF)

## ■ AUTHOR INFORMATION


### Corresponding Author

**Md. Aminur Rahman** − *Global Centre for Environmental Remediation (GCER), College of Engineering, Science and Environment, The University of Newcastle, Callaghan, New South Wales 2308, Australia; Department of Public Health Engineering (DPHE), Zonal Laboratory, Khulna 9100, Bangladesh;* orcid.org/0000-0003-4741-2507; Email: md.aminur.rahman@uon.edu.au

### Authors

**Dane Lamb** − *Chemical and Environmental Engineering, School of Engineering, RMIT University, Melbourne, Victoria 3000, Australia;* orcid.org/0000-0003-2303-5460

**Mohammad Mahmudur Rahman** − *Global Centre for Environmental Remediation (GCER), College of Engineering, Science and Environment, The University of Newcastle, Callaghan, New South Wales 2308, Australia;* orcid.org/0000-0002-3426-5221

**Md Mezbaul Bahar** − *Global Centre for Environmental Remediation (GCER), College of Engineering, Science and Environment, The University of Newcastle, Callaghan, New South Wales 2308, Australia*

**Peter Sanderson** − *Global Centre for Environmental Remediation (GCER), College of Engineering, Science and Environment, The University of Newcastle, Callaghan, New South Wales 2308, Australia;* orcid.org/0000-0001-8545-4260

Complete contact information is available at: https://pubs.acs.org/10.1021/acsomega.1c04129


### Author Contributions

M.A.R.: conceptualization, methodology, data curation, formal analysis, and writing-original draft; D.L.: conceptualization, reviewing, editing, resources, and supervision; M.M.R.: reviewing, editing, and supervision; M.M.B.: reviewing, editing, and supervision; and P.S.: reviewing, editing, and supervision.

### Notes

The authors declare no competing financial interest.

## ■ ACKNOWLEDGMENTS

First author is grateful to The University of Newcastle, Australia for providing UNIPRS and UNRSC central scholarship and to the Department of Public Health Engineering (DPHE), Bangladesh for granting leave for PhD study. The authors are thankful to the EMX unit at The University of Newcastle, Australia for using the analytical support of XRD, SEM, and TEM-EDS. We also thank Dr Bill Gong of the Mark Wainwright Analytical Centre located at the University of New South Wales for assistance with XPS analysis. We also greatly acknowledged the funding support from the Cooperative Research Centre for Contamination Assessment and Remediation of the Environment (CRC-CARE) for XPS analysis and CRC for High Performance Soils (HPS) for providing completion scholarship to the first author.

## ■ REFERENCES


(1) International Agency for Research on Cancer. Arsenic in drinking-water. In *IARC Monographs on the Evaluation of Carcinogenic Risks to Humans, Some Drinking-Water Disinfectants and Contaminants, Including Arsenic*; World Health Organization-International Agency for Research on Cancer: Lyon, 2001; Vol. *84*, pp 39−270.

(2) Fendorf, S.; Michael, H. A.; van Geen, A. Spatial and temporal variations of groundwater arsenic in South and Southeast Asia. *Science* **2010**, *328*, 1123−1127.

(3) Smedley, P. L.; Kinniburgh, D. G. A review of the source, behaviour and distribution of arsenic in natural waters. *Appl. Geochem.* **2002**, *17*, 517−568.

(4) Rodríguez-Lado, L.; Sun, G.; Berg, M.; Zhang, Q.; Xue, H.; Zheng, Q.; Johnson, C. A. Groundwater arsenic contamination throughout China. *Science* **2013**, *341*, 866−868.

(5) Smedley, P. L.; Kinniburgh, D. G. A review of the source, behaviour and distribution of arsenic in natural waters. *Appl. Geochem.* **2002**, *17*, 517−568.

(6) Oremland, R. S.; Stolz, J. F. The ecology of arsenic. *Science* **2003**, *300*, 939−944.

(7) Chakraborti, D.; Singh, S. K.; Rashid, M. H.; Rahman, M. M. Arsenic: occurrence in groundwater. *Encyclopedia of Environmental Health*; Elsevier, 2018; pp 165−180.

(8) World Health Organization. *Guidelines for drinking-water quality: incorporating the1st addendum*; World Health Organization: Geneva, 2017; p 415.

(9) Rahman, M. M.; Ng, J. C.; Naidu, R. Chronic exposure of arsenic via drinking water and its adverse health impacts on humans. *Environ. Geochem. Health* **2009**, *31*, 189−200.

(10) Gupta, R.; Kumar, P.; Fahmi, N.; Garg, B.; Dutta, S.; Sachar, S.; Matharu, A. S.; Vimaleswaran, K. S. Endocrine disruption and obesity: A current review on environmental obesogens. *Cur. Res. Green Sustain. Chem.* **2020**, *3*, 100009.

(11) Xu, L.; Suman, S.; Sharma, P.; Kumar, R.; Singh, S. K.; Bose, N.; Ghosh, A.; Rahman, M. M.; Polya, D. A.; Mondal, D. Assessment of hypertension association with arsenic exposure from food and drinking water in Bihar, India. *Ecotoxicol. Environ. Saf.* **2021**, *223*, 112572.

(12) He, X.; Deng, F.; Shen, T.; Yang, L.; Chen, D.; Luo, J.; Luo, X.; Min, X.; Wang, F. Exceptional adsorption of arsenic by zirconium metal-organic frameworks: Engineering exploration and mechanism insight. *J. Colloid Interface Sci.* **2019**, *539*, 223−234.

(13) Rahman, M. A.; Lamb, D.; Rahman, M. M.; Bahar, M. M.; Sanderson, P.; Abbasi, S.; Bari, A. F.; Naidu, R. Removal of arsenate from contaminated waters by novel zirconium and zirconium-iron modified biochar. *J. Hazard. Mater.* **2021**, *409*, 124488.

(14) Niazi, N. K.; Bibi, I.; Shahid, M.; Ok, Y. S.; Burton, E. D.; Wang, H.; Shaheen, S. M.; Rinklebe, J.; Lüttge, A. Arsenic removal by perilla leaf biochar in aqueous solutions and groundwater: an integrated spectroscopic and microscopic examination. *Environ. Pollut.* **2018**, *232*, 31−41.

(15) Nidheesh, P. V.; Singh, T. S. A. Arsenic removal by electrocoagulation process: Recent trends and removal mechanism. *Chemosphere* **2017**, *181*, 418−432.

(16) Víctor-Ortega, M. D.; Ratnaweera, H. C. Double filtration as an effective system for removal of arsenate and arsenite from drinking water through reverse osmosis. *Process Saf. Environ. Prot.* **2017**, *111*, 399−408.

(17) He, Y.; Tang, Y. P.; Ma, D.; Chung, T.-S. UiO-66 incorporated thin-film nanocomposite membranes for efficient selenium and arsenic removal. *J. Membr. Sci.* **2017**, *541*, 262−270.

(18) Dutta, P. K.; Pehkonen, S. O.; Sharma, V. K.; Ray, A. K. Photocatalytic oxidation of arsenic (III): evidence of hydroxyl radicals. *Environ. Sci. Technol.* **2005**, *39*, 1827−1834.
(19) Jia, Y.; Xu, L.; Fang, Z.; Demopoulos, G. P. Observation of surface precipitation of arsenate on ferrihydrite. *Environ. Sci. Technol.* **2006**, *40*, 3248−3253.
(20) Liu, X.; Pang, H.; Liu, X.; Li, Q.; Zhang, N.; Mao, L.; Qiu, M.; Hu, B.; Yang, H.; Wang, X. Orderly porous covalent organic frameworks-based materials: superior adsorbents for pollutants removal from aqueous solutions. *The Innovation* **2021**, *2*, 100076.
(21) Lin, L.; Qiu, W.; Wang, D.; Huang, Q.; Song, Z.; Chau, H. W. Arsenic removal in aqueous solution by a novel Fe-Mn modified biochar composite: characterization and mechanism. *Ecotoxicol. Environ. Saf.* **2017**, *144*, 514−521.
(22) Sahu, N.; Singh, J.; Koduru, J. R. Removal of arsenic from aqueous solution by novel iron and iron−zirconium modified activated carbon derived from chemical carbonization of Tectona grandis sawdust: Isotherm, kinetic, thermodynamic and breakthrough curve modelling. *Environ. Res.* **2021**, *200*, 111431.
(23) Mohapatra, D.; Mishra, D.; Chaudhury, G. R.; Das, R. P. Arsenic adsorption mechanism on clay minerals and its dependence on temperature. *Korean J. Chem. Eng.* **2007**, *24*, 426−430.
(24) Foroutan, R.; Mohammadi, R.; Adeleye, A. S.; Farjadfard, S.; Esvandi, Z.; Arfaeinia, H.; Sorial, G. A.; Ramavandi, B.; Sahebi, S. Efficient arsenic (V) removal from contaminated water using natural clay and clay composite adsorbents. *Environ. Sci. Pollut. Res.* **2019**, *26*, 29748−29762.
(25) Manning, B. A.; Goldberg, S. Adsorption and stability of arsenic (III) at the clay mineral− water interface. *Environ. Sci. Technol.* **1997**, *31*, 2005−2011.
(26) Pawar, R. R.; Lalhmunsiama, M.; Kim, M.; Kim, J.-G.; Hong, S.-M.; Sawant, S. Y.; Lee, S. M. Efficient removal of hazardous lead, cadmium, and arsenic from aqueous environment by iron oxide modified clay-activated carbon composite beads. *Appl. Clay Sci.* **2018**, *162*, 339−350.
(27) Han, C.; Li, H.; Pu, H.; Yu, H.; Deng, L.; Huang, S.; Luo, Y. Synthesis and characterization of mesoporous alumina and their performances for removing arsenic (V). *Chem. Eng. J.* **2013**, *217*, 1−9.
(28) Kim, Y.; Kim, C.; Choi, I.; Rengaraj, S.; Yi, J. Arsenic removal using mesoporous alumina prepared via a templating method. *Environ. Sci. Technol.* **2004**, *38*, 924−931.
(29) Saha, S.; Sarkar, P. Arsenic remediation from drinking water by synthesized nano-alumina dispersed in chitosan-grafted polyacrylamide. *J. Hazard. Mater.* **2012**, *227−228*, 68−78.
(30) Chen, W.; Parette, R.; Zou, J.; Cannon, F. S.; Dempsey, B. A. Arsenic removal by iron-modified activated carbon. *Water Res.* **2007**, *41*, 1851−1858.
(31) Zhu, H.; Jia, Y.; Wu, X.; Wang, H. Removal of arsenic from water by supported nano zero-valent iron on activated carbon. *J. Hazard. Mater.* **2009**, *172*, 1591−1596.
(32) Hassan, A. F.; Abdel-Mohsen, A. M.; Elhadidy, H. Adsorption of arsenic by activated carbon, calcium alginate and their composite beads. *Int. J. Biol. Macromol.* **2014**, *68*, 125−130.
(33) Das, T. K.; Sakthivel, T. S.; Jeyaranjan, A.; Seal, S.; Bezbaruah, A. N. Ultra-high arsenic adsorption by graphene oxide iron nanohybrid: removal mechanisms and potential applications. *Chemosphere* **2020**, *253*, 126702.
(34) Vithanage, M.; Herath, I.; Joseph, S.; Bundschuh, J.; Bolan, N.; Ok, Y. S.; Kirkham, M. B.; Rinklebe, J. Interaction of arsenic with biochar in soil and water: a critical review. *Carbon* **2017**, *113*, 219−230.
(35) Imran, M.; Iqbal, M. M.; Iqbal, J.; Shah, N. S.; Khan, Z. U. H.; Murtaza, B.; Amjad, M.; Ali, S.; Rizwan, M. Synthesis, characterization and application of novel MnO and CuO impregnated biochar composites to sequester arsenic (As) from water: modeling, thermodynamics and reusability. *J. Hazard. Mater.* **2021**, *401*, 123338.
(36) Mukherjee, S.; Thakur, A. K.; Goswami, R.; Mazumder, P.; Taki, K.; Vithanage, M.; Kumar, M. Efficacy of agricultural waste derived biochar for arsenic removal: Tackling water quality in the Indo-Gangetic plain. *J. Environ. Manage.* **2021**, *281*, 111814.
(37) Niazi, N. K.; Bibi, I.; Shahid, M.; Ok, Y. S.; Shaheen, S. M.; Rinklebe, J.; Wang, H.; Murtaza, B.; Islam, E.; Farrakh Nawaz, M.; Lüttge, A. Arsenic removal by Japanese oak wood biochar in aqueous solutions and well water: Investigating arsenic fate using integrated spectroscopic and microscopic techniques. *Sci. Total Environ.* **2018**, *621*, 1642−1651.
(38) Mohan, D.; Sarswat, A.; Ok, Y. S.; Pittman, C. U., Jr Organic and inorganic contaminants removal from water with biochar, a renewable, low cost and sustainable adsorbent−a critical review. *Bioresour. Technol.* **2014**, *160*, 191−202.
(39) Hu, B.; Ai, Y.; Jin, J.; Hayat, T.; Alsaedi, A.; Zhuang, L.; Wang, X. Efficient elimination of organic and inorganic pollutants by biochar and biochar-based materials. *Biochar* **2020**, *2*, 47−64.
(40) Liang, L.; Xi, F.; Tan, W.; Meng, X.; Hu, B.; Wang, X. Review of organic and inorganic pollutants removal by biochar and biochar-based composites. *Biochar* **2021**, *3*, 255.
(41) Zhou, Z.; Liu, Y.-g.; Liu, S.-b.; Liu, H.-y.; Zeng, G.-m.; Tan, X.-f.; Yang, C.-p.; Ding, Y.; Yan, Z.-l.; Cai, X.-x. Sorption performance and mechanisms of arsenic (V) removal by magnetic gelatin-modified biochar. *Chem. Eng. J.* **2017**, *314*, 223−231.
(42) Zhang, Y.; Fan, J.; Fu, M.; Ok, Y. S.; Hou, Y.; Cai, C. Adsorption antagonism and synergy of arsenate (V) and cadmium (II) onto Fe-modified rice straw biochars. *Environ. Geochem. Health* **2019**, *41*, 1755−1766.
(43) Agrafioti, E.; Kalderis, D.; Diamadopoulos, E. Ca and Fe modified biochars as adsorbents of arsenic and chromium in aqueous solutions. *J. Environ. Manage.* **2014**, *146*, 444−450.
(44) Wang, S.; Gao, B.; Li, Y. Enhanced arsenic removal by biochar modified with nickel (Ni) and manganese (Mn) oxyhydroxides. *J. Ind. Eng. Chem.* **2016**, *37*, 361−365.
(45) Wang, S.; Gao, B.; Li, Y.; Mosa, A.; Zimmerman, A. R.; Ma, L. Q.; Harris, W. G.; Migliaccio, K. W. Manganese oxide-modified biochars: preparation, characterization, and sorption of arsenate and lead. *Bioresour. Technol.* **2015**, *181*, 13−17.
(46) Rahman, M. A.; Lamb, D.; Rahman, M. M.; Bahar, M. M.; Sanderson, P.; Abbasi, S.; Bari, A. S. M. F.; Naidu, R. Removal of arsenate from contaminated waters by novel zirconium and zirconium-iron modified biochar. *J. Hazard. Mater.* **2021**, *409*, 124488.
(47) Kalaruban, M.; Loganathan, P.; Nguyen, T. V.; Nur, T.; Hasan Johir, M. A.; Nguyen, T. H.; Trinh, M. V.; Vigneswaran, S. Iron-impregnated granular activated carbon for arsenic removal: application to practical column filters. *J. Environ. Manage.* **2019**, *239*, 235−243.
(48) Iqbal, J.; Shah, N. S.; Sayed, M.; Imran, M.; Muhammad, N.; Howari, F. M.; Alkhoori, S. A.; Khan, J. A.; Haq Khan, Z. U.; Bhatnagar, A.; Polychronopoulou, K.; Ismail, I.; Haija, M. A. Synergistic effects of activated carbon and nano-zerovalent copper on the performance of hydroxyapatite-alginate beads for the removal of As3+ from aqueous solution. *J. Cleaner Prod.* **2019**, *235*, 875−886.
(49) Zhang, G.; Liu, F.; Liu, H.; Qu, J.; Liu, R. Respective role of Fe and Mn oxide contents for arsenic sorption in iron and manganese binary oxide: an X-ray absorption spectroscopy investigation. *Environ. Sci. Technol.* **2014**, *48*, 10316−10322.
(50) Su, C.; Puls, R. W. Arsenate and arsenite removal by zerovalent iron: kinetics, redox transformation, and implications for in situ groundwater remediation. *Environ. Sci. Technol.* **2001**, *35*, 1487−1492.
(51) Nguyen, T. T. Q.; Loganathan, P.; Nguyen, T. V.; Vigneswaran, S.; Ngo, H. H. Iron and zirconium modified luffa fibre as an effective bioadsorbent to remove arsenic from drinking water. *Chemosphere* **2020**, *258*, 127370.
(52) Chen, A. S. C.; Sorg, T. J.; Wang, L. Regeneration of iron-based adsorptive media used for removing arsenic from groundwater. *Water Res.* **2015**, *77*, 85−97.
(53) Yuan, Z.; Zhang, G.; Lin, J.; Zeng, X.; Ma, X.; Wang, X.; Wang, S.; Jia, Y. The stability of Fe (III)-As (V) co-precipitate in the


https://doi.org/10.1021/acsomega.1c04129
*ACS Omega* 2022, 7, 101−117

presence of ascorbic acid: Effect of pH and Fe/As molar ratio. *Chemosphere* **2019**, *218*, 670−679.
(54) Zhang, D.; Wang, S.; Gomez, M. A.; Wang, Y.; Jia, Y. The long-term stability of FeIII-AsV coprecipitates at pH 4 and 7: mechanisms controlling the arsenic behavior. *J. Hazard. Mater.* **2019**, *374*, 276−286.
(55) Berg, M.; Tran, H. C.; Nguyen, T. C.; Pham, H. V.; Schertenleib, R.; Giger, W. Arsenic contamination of groundwater and drinking water in Vietnam: a human health threat. *Environ. Sci. Technol.* **2001**, *35*, 2621−2626.
(56) Berg, M.; Trang, P. T. K.; Stengel, C.; Buschmann, J.; Viet, P. H.; Van Dan, N.; Giger, W.; Stüben, D. Hydrological and sedimentary controls leading to arsenic contamination of groundwater in the Hanoi area, Vietnam: the impact of iron-arsenic ratios, peat, river bank deposits, and excessive groundwater abstraction. *Chem. Geol.* **2008**, *249*, 91−112.
(57) Fakhreddine, S.; Prommer, H.; Gorelick, S. M.; Dadakis, J.; Fendorf, S. Controlling arsenic mobilization during managed aquifer recharge: The role of sediment heterogeneity. *Environ. Sci. Technol.* **2020**, *54*, 8728−8738.
(58) Nur, T.; Loganathan, P.; Ahmed, M. B.; Johir, M. A. H.; Nguyen, T. V.; Vigneswaran, S. Removing arsenic from water by coprecipitation with iron: effect of arsenic and iron concentrations and adsorbent incorporation. *Chemosphere* **2019**, *226*, 431−438.
(59) Hong, H.-J.; Farooq, W.; Yang, J.-S.; Yang, J.-W. Preparation and evaluation of Fe-Al binary oxide for arsenic removal: comparative study with single metal oxides. *Sep. Sci. Technol.* **2010**, *45*, 1975−1981.
(60) Zhang, G.; Ren, Z.; Zhang, X.; Chen, J. Nanostructured iron (III)-copper (II) binary oxide: a novel adsorbent for enhanced arsenic removal from aqueous solutions. *Water Res.* **2013**, *47*, 4022−4031.
(61) Xu, W.; Wang, H.; Liu, R.; Zhao, X.; Qu, J. Arsenic release from arsenic-bearing Fe−Mn binary oxide: Effects of Eh condition. *Chemosphere* **2011**, *83*, 1020−1027.
(62) Qi, J.; Zhang, G.; Li, H. Efficient removal of arsenic from water using a granular adsorbent: Fe−Mn binary oxide impregnated chitosan bead. *Bioresour. Technol.* **2015**, *193*, 243−249.
(63) Liu, S.; Kang, S.; Wang, G.; Zhao, H.; Cai, W. Micro/nanostructured porous Fe−Ni binary oxide and its enhanced arsenic adsorption performances. *J. Colloid Interface Sci.* **2015**, *458*, 94−102.
(64) Wang, S.; Gao, B.; Li, Y.; Zimmerman, A. R.; Cao, X. Sorption of arsenic onto Ni/Fe layered double hydroxide (LDH)-biochar composites. *RSC Adv.* **2016**, *6*, 17792−17799.
(65) Dou, X.; Wang, G.-C.; Zhu, M.; Liu, F.; Li, W.; Mohan, D.; Pittman, C. U., Jr Identification of Fe and Zr oxide phases in an iron-zirconium binary oxide and arsenate complexes adsorbed onto their surfaces. *J. Hazard. Mater.* **2018**, *353*, 340−347.
(66) Ren, Z.; Zhang, G.; Paul Chen, J. Adsorptive removal of arsenic from water by an iron−zirconium binary oxide adsorbent. *J. Colloid Interface Sci.* **2011**, *358*, 230−237.
(67) Zhang, J.; Chen, N.; Feng, C.; Li, M.; Lv, L.; Hu, Q. Chemical regeneration mechanism of Fe-impregnated chitosan using ferric chloride. *RSC Adv.* **2015**, *5*, 77610−77618.
(68) Tang, W.; Su, Y.; Li, Q.; Gao, S.; Shang, J. K. Superparamagnetic magnesium ferrite nanoadsorbent for effective arsenic (III, V) removal and easy magnetic separation. *Water Res.* **2013**, *47*, 3624−3634.
(69) Amen, R.; Bashir, H.; Bibi, I.; Shaheen, S. M.; Niazi, N. K.; Shahid, M.; Hussain, M. M.; Antoniadis, V.; Shakoor, M. B.; Al-Solaimani, S. G.; Wang, H.; Bundschuh, J.; Rinklebe, J. A critical review on arsenic removal from water using biochar-based sorbents: The significance of modification and redox reactions. *Chem. Eng. J.* **2020**, *396*, 125195.
(70) Gupta, K.; Biswas, K.; Ghosh, U. C. Nanostructure iron (III)−zirconium (IV) binary mixed oxide: synthesis, characterization, and physicochemical aspects of arsenic (III) sorption from the aqueous solution. *Ind. Eng. Chem. Res.* **2008**, *47*, 9903−9912.
(71) Stumm, W. *Chemistry of the Solid−Water Interface: Processes at the Mineral−Water and Particle−Water Interface in Natural Systems*; John Wiley & Son Inc., 1992.
(72) Kingston, F. J.; Posner, A. M.; Quirk, J. P. Anion adsorption by goethite and gibbsite: I. The role of the proton in determining adsorption envelopes. *J. Soil Sci.* **1972**, *23*, 177−192.
(73) Zhang, G.; Liu, H.; Liu, R.; Qu, J. Removal of phosphate from water by a Fe−Mn binary oxide adsorbent. *J. Colloid Interface Sci.* **2009**, *335*, 168−174.
(74) Hu, B.; Wang, H.; Liu, R.; Qiu, M. Highly efficient U (VI) capture by amidoxime/carbon nitride composites: Evidence of EXAFS and modeling. *Chemosphere* **2021**, *274*, 129743.
(75) Liu, F.; Hua, S.; Wang, C.; Qiu, M.; Jin, L.; Hu, B. Adsorption and reduction of Cr (VI) from aqueous solution using cost-effective caffeic acid functionalized corn starch. *Chemosphere* **2021**, *279*, 130539.
(76) Liu, C.-H.; Chuang, Y.-H.; Chen, T.-Y.; Tian, Y.; Li, H.; Wang, M.-K.; Zhang, W. Mechanism of arsenic adsorption on magnetite nanoparticles from water: thermodynamic and spectroscopic studies. *Environ. Sci. Technol.* **2015**, *49*, 7726−7734.
(77) Liu, D.; Deng, S.; Maimaiti, A.; Wang, B.; Huang, J.; Wang, Y.; Yu, G. As (III) and As (V) adsorption on nanocomposite of hydrated zirconium oxide coated carbon nanotubes. *J. Colloid Interface Sci.* **2018**, *511*, 277−284.
(78) Abid, M.; Niazi, N. K.; Bibi, I.; Farooqi, A.; Ok, Y. S.; Kunhikrishnan, A.; Ali, F.; Ali, S.; Igalavithana, A. D.; Arshad, M. Arsenic (V) biosorption by charred orange peel in aqueous environments. *Int. J. Phytorem.* **2016**, *18*, 442−449.
(79) Feng, N.; Guo, X.; Liang, S.; Zhu, Y.; Liu, J. Biosorption of heavy metals from aqueous solutions by chemically modified orange peel. *J. Hazard. Mater.* **2011**, *185*, 49−54.
(80) Shakoor, M. B.; Niazi, N. K.; Bibi, I.; Shahid, M.; Saqib, Z. A.; Nawaz, M. F.; Shaheen, S. M.; Wang, H.; Tsang, D. C. W.; Bundschuh, J.; Ok, Y. S.; Rinklebe, J. Exploring the arsenic removal potential of various biosorbents from water. *Environ. Int.* **2019**, *123*, 567−579.
(81) Kizito, S.; Wu, S.; Kipkemoi Kirui, W.; Lei, M.; Lu, Q.; Bah, H.; Dong, R. Evaluation of slow pyrolyzed wood and rice husks biochar for adsorption of ammonium nitrogen from piggery manure anaerobic digestate slurry. *Sci. Total Environ.* **2015**, *505*, 102−112.
(82) Xu, Z.; Wan, Z.; Sun, Y.; Cao, X.; Hou, D.; Alessi, D. S.; Ok, Y. S.; Tsang, D. C. W. Unraveling Iron Speciation on Fe-biochar with Distinct Arsenic Removal Mechanisms and Depth Distributions of As and Fe. *Chem. Eng. J.* **2021**, *425*, 131489.
(83) Merle-Méjean, T.; Barberis, P.; Othmane, S. B.; Nardou, F.; Quintard, P. E. Chemical forms of hydroxyls on/in zirconia: An FT-IR study. *J. Eur. Ceram. Soc.* **1998**, *18*, 1579−1586.
(84) Zhou, W.; Ma, Z.; Guo, S.; Wang, M.; Wang, J.; Xia, M.; Jia, L.; Hou, B.; Li, D.; Zhao, Y. Comparative study of CO adsorption on zirconia polymorphs with DRIFT and transmission FT-IR spectroscopy. *Appl. Surf. Sci.* **2018**, *427*, 867−873.
(85) Rahman, M. A.; Rahman, M. M.; Bahar, M. M.; Sanderson, P.; Lamb, D. Antimonate sequestration from aqueous solution using zirconium, iron and zirconium-iron modified biochars. *Sci. Rep.* **2021**, *11*, 8113.
(86) Goldberg, S.; Johnston, C. T. Mechanisms of arsenic adsorption on amorphous oxides evaluated using macroscopic measurements, vibrational spectroscopy, and surface complexation modeling. *J. Colloid Interface Sci.* **2001**, *234*, 204−216.
(87) Cerrato, G.; Bordiga, S.; Barbera, S.; Morterra, C. Surface characterization of monoclinic ZrO2: I. Morphology, FTIR spectral features, and computer modelling. *Appl. Surf. Sci.* **1997**, *115*, 53−65.
(88) Jung, K. T.; Bell, A. T. The effects of synthesis and pretreatment conditions on the bulk structure and surface properties of zirconia. *J. Mol. Catal. A: Chem.* **2000**, *163*, 27−42.
(89) Chang, Q.; Lin, W.; Ying, W. C. Preparation of iron-impregnated granular activated carbon for arsenic removal from drinking water. *J. Hazard. Mater.* **2010**, *184*, 515−522.


https://doi.org/10.1021/acsomega.1c04129
*ACS Omega* 2022, 7, 101−117

(90) Jang, M.; Chen, W.; Cannon, F. S. Preloading hydrous ferric oxide into granular activated carbon for arsenic removal. *Environ. Sci. Technol.* **2008**, *42*, 3369−3374.
(91) Yin, H.; Kong, M.; Gu, X.; Chen, H. Removal of arsenic from water by porous charred granulated attapulgite-supported hydrated iron oxide in bath and column modes. *J. Cleaner Prod.* **2017**, *166*, 88−97.
(92) Wang, X.; Pan, S.; Zhang, M.; Qi, J.; Sun, X.; Gu, C.; Wang, L.; Li, J. Modified hydrous zirconium oxide/PAN nanofibers for efficient defluoridation from groundwater. *Sci. Total Environ.* **2019**, *685*, 401−409.
(93) Marakatti, V. S.; Marappa, S.; Gaigneaux, E. M. Sulfated zirconia: an efficient catalyst for the Friedel−Crafts monoalkylation of resorcinol with methyl tertiary butyl ether to 4-tertiary butylresorcinol. *New J. Chem.* **2019**, *43*, 7733−7742.
(94) Ding, M.; De Jong, B. H. W. S.; Roosendaal, S. J.; Vredenberg, A. XPS studies on the electronic structure of bonding between solid and solutes: adsorption of arsenate, chromate, phosphate, Pb2+, and Zn2+ ions on amorphous black ferric oxyhydroxide. *Geochim. Cosmochim. Acta* **2000**, *64*, 1209−1219.
(95) Hu, X.; Ding, Z.; Zimmerman, A. R.; Wang, S.; Gao, B. Batch and column sorption of arsenic onto iron-impregnated biochar synthesized through hydrolysis. *Water Res.* **2015**, *68*, 206−216.
(96) Frau, F.; Biddau, R.; Fanfani, L. Effect of major anions on arsenate desorption from ferrihydrite-bearing natural samples. *Appl. Geochem.* **2008**, *23*, 1451−1466.
(97) Schmidt, M. P.; Siciliano, S. D.; Peak, D. Spectroscopic Quantification of Inner-and Outer-Sphere Oxyanion Complexation Kinetics: Ionic Strength and Background Cation Effect on Sulfate Adsorption to Hematite. *ACS Earth Space Chem.* **2020**, *4*, 1765−1776.
(98) Mendez, J. C.; Hiemstra, T. Carbonate adsorption to ferrihydrite: Competitive interaction with phosphate for use in soil systems. *ACS Earth Space Chem.* **2018**, *3*, 129−141.
(99) Kolbe, F.; Weiss, H.; Morgenstern, P.; Wennrich, R.; Lorenz, W.; Schurk, K.; Stanjek, H.; Daus, B. Sorption of aqueous antimony and arsenic species onto akaganeite. *J. Colloid Interface Sci.* **2011**, *357*, 460−465.
(100) Khare, N.; Hesterberg, D.; Martin, J. D. XANES investigation of phosphate sorption in single and binary systems of iron and aluminum oxide minerals. *Environ. Sci. Technol.* **2005**, *39*, 2152−2160.
(101) Sigdel, A.; Park, J.; Kwak, H.; Park, P.-K. Arsenic removal from aqueous solutions by adsorption onto hydrous iron oxide-impregnated alginate beads. *J. Ind. Eng. Chem.* **2016**, *35*, 277−286.
(102) Verma, L.; Singh, J. Synthesis of novel biochar from waste plant litter biomass for the removal of Arsenic (III and V) from aqueous solution: A mechanism characterization, kinetics and thermodynamics. *J. Environ. Manage.* **2019**, *248*, 109235.
(103) Persson, R. A. X.; Pattni, V.; Singh, A.; Kast, S. M.; Heyden, M. Signatures of solvation thermodynamics in spectra of intermolecular vibrations. *J. Chem. Theory Comput.* **2017**, *13*, 4467−4481.
(104) Dragan, A. I.; Read, C. M.; Crane-Robinson, C. Enthalpy−entropy compensation: the role of solvation. *Eur. Biophys. J.* **2017**, *46*, 301−308.
(105) Safi, S. R.; Senmoto, K.; Gotoh, T.; Iizawa, T.; Nakai, S. The effect of γ-FeOOH on enhancing arsenic adsorption from groundwater with DMApAAQ+ FeOOH gel composite. *Sci. Rep.* **2019**, *9*, 11909.
(106) Ali, S.; Rizwan, M.; Shakoor, M. B.; Jilani, A.; Anjum, R. High sorption efficiency for As (III) and As (V) from aqueous solutions using novel almond shell biochar. *Chemosphere* **2020**, *243*, 125330.
(107) Cruz, G. J. F.; Mondal, D.; Rimaycuna, J.; Soukup, K.; Gómez, M. M.; Solis, J. L.; Lang, J. Agrowaste derived biochars impregnated with ZnO for removal of arsenic and lead in water. *J. Environ. Chem. Eng.* **2020**, *8*, 103800.
(108) Nham, N. T.; Tahtamouni, T. M. A.; Nguyen, T. D.; Huong, P. T.; Jitae, K.; Viet, N. M.; Noi, N. V.; Phuong, N. M.; Anh, N. T. H. Synthesis of iron modified rice straw biochar toward arsenic from groundwater. *Mater. Res. Express* **2019**, *6*, 115528.
(109) Wu, C.; Huang, L.; Xue, S.-G.; Huang, Y.-Y.; Hartley, W.; Cui, M.-q.; Wong, M.-H. Arsenic sorption by red mud-modified biochar produced from rice straw. *Environ. Sci. Pollut. Res.* **2017**, *24*, 18168−18178.
(110) Yan, J.; Xue, Y.; Long, L.; Zeng, Y.; Hu, X. Adsorptive removal of As (V) by crawfish shell biochar: batch and column tests. *Environ. Sci. Pollut. Res.* **2018**, *25*, 34674−34683.
(111) Chunhui, L.; Jin, T.; Puli, Z.; Bin, Z.; Duo, B.; Xuebin, L. Simultaneous removal of fluoride and arsenic in geothermal water in Tibet using modified yak dung biochar as an adsorbent. *R. Soc. Open Sci.* **2018**, *5*, 181266.
(112) He, R.; Peng, Z.; Lyu, H.; Huang, H.; Nan, Q.; Tang, J. Synthesis and characterization of an iron-impregnated biochar for aqueous arsenic removal. *Sci. Total Environ.* **2018**, *612*, 1177−1186.
(113) Alam, M. A.; Shaikh, W. A.; Alam, M. O.; Bhattacharya, T.; Chakraborty, S.; Show, B.; Saha, I. Adsorption of As (III) and As (V) from aqueous solution by modified Cassia fistula (golden shower) biochar. *Appl. Water Sci.* **2018**, *8*, 198.
(114) Bakshi, S.; Banik, C.; Rathke, S. J.; Laird, D. A. Arsenic sorption on zero-valent iron-biochar complexes. *Water Res.* **2018**, *137*, 153−163.
(115) Yoon, K.; Cho, D.-W.; Tsang, D. C. W.; Bolan, N.; Rinklebe, J.; Song, H. Fabrication of engineered biochar from paper mill sludge and its application into removal of arsenic and cadmium in acidic water. *Bioresour. Technol.* **2017**, *246*, 69−75.
(116) Norazlina, A. S.; Che, F. I.; Rosenani, A. B. Characterization of oil palm empty fruit bunch and rice husk biochars and their potential to adsorb arsenic and cadmium. *Am. J. Agric. Biol. Sci.* **2014**, *9*, 450−456.
(117) Agrafioti, E.; Kalderis, D.; Diamadopoulos, E. Arsenic and chromium removal from water using biochars derived from rice husk, organic solid wastes and sewage sludge. *J. Environ. Manage.* **2014**, *133*, 309−314.
(118) Samsuri, A. W.; Sadegh-Zadeh, F.; Seh-Bardan, B. J. Adsorption of As (III) and As (V) by Fe coated biochars and biochars produced from empty fruit bunch and rice husk. *J. Environ. Chem. Eng.* **2013**, *1*, 981−988.
(119) Zhu, N.; Yan, T.; Qiao, J.; Cao, H. Adsorption of arsenic, phosphorus and chromium by bismuth impregnated biochar: Adsorption mechanism and depleted adsorbent utilization. *Chemosphere* **2016**, *164*, 32−40.
(120) Zhang, F.; Wang, X.; Xionghui, J.; Ma, L. Efficient arsenate removal by magnetite-modified water hyacinth biochar. *Environ. Pollut.* **2016**, *216*, 575−583.
(121) Peng, Y.; Azeem, M.; Li, R.; Xing, L.; Li, Y.; Zhang, Y.; Guo, Z.; Wang, Q.; Ngo, H. H.; Qu, G.; Zhang, Z. Zirconium hydroxide nanoparticle encapsulated magnetic biochar composite derived from rice residue: Application for As (III) and As (V) polluted water purification. *J. Hazard. Mater.* **2022**, *423*, 127081.
(122) Johnston, S. G.; Bennett, W. W.; Doriean, N.; Hockmann, K.; Karimian, N.; Burton, E. D. Antimony and arsenic speciation, redox-cycling and contrasting mobility in a mining-impacted river system. *Sci. Total Environ.* **2020**, *710*, 136354.
(123) Zhu, Y.; He, X.; Xu, J.; Fu, Z.; Wu, S.; Ni, J.; Hu, B. Insight into efficient removal of Cr (VI) by magnetite immobilized with Lysinibacillus sp. JLT12: Mechanism and performance. *Chemosphere* **2021**, *262*, 127901.
(124) Pinakidou, F.; Katsikini, M.; Simeonidis, K.; Kaprara, E.; Paloura, E. C.; Mitrakas, M. On the passivation mechanism of Fe3O4 nanoparticles during Cr (VI) removal from water: a XAFS study. *Appl. Surf. Sci.* **2016**, *360*, 1080−1086.
(125) Grosvenor, A. P.; Kobe, B. A.; Biesinger, M. C.; McIntyre, N. S. Investigation of multiplet splitting of Fe 2p XPS spectra and bonding in iron compounds. *Surf. Interface Anal.* **2004**, *36*, 1564−1574.
(126) Descostes, M.; Mercier, F.; Thromat, N.; Beaucaire, C.; Gautier-Soyer, M. Use of XPS in the determination of chemical environment and oxidation state of iron and sulfur samples: constitution of a data basis in binding energies for Fe and S reference


https://doi.org/10.1021/acsomega.1c04129
*ACS Omega* 2022, 7, 101−117

compounds and applications to the evidence of surface species of an oxidized pyrite in a carbonate medium. *Appl. Surf. Sci.* **2000**, *165*, 288−302.
(127) Kwon Jeong, I.; Mahadik, M. A.; Kim, S.; Pathan, H. M.; Chae, W.-S.; Suk Chung, H.; Won Kong, G.; Hee Choi, S.; Suk Jang, J. Transparent zirconium-doped hematite nanocoral photoanode via in-situ diluted hydrothermal approach for efficient solar water splitting. *Chem. Eng. J.* **2020**, *390*, 124504.
(128) Uz-Zaman, K. A.; Biswas, B.; Rahman, M. M.; Naidu, R. Smectite-supported chain of iron nanoparticle beads for efficient clean-up of arsenate contaminated water. *J. Hazard. Mater.* **2021**, *407*, 124396.
(129) Navarathna, C. M.; Karunanayake, A. G.; Gunatilake, S. R.; Pittman, C. U., Jr; Perez, F.; Mohan, D.; Mlsna, T. Removal of Arsenic (III) from water using magnetite precipitated onto Douglas fir biochar. *J. Environ. Manage.* **2019**, *250*, 109429.
(130) Fang, Z.; Deng, Z.; Liu, A.; Zhang, X.; Lv, L.; Pan, B. Enhanced removal of arsenic from water by using sub-10 nm hydrated zirconium oxides confined inside gel-type anion exchanger. *J. Hazard. Mater.* **2021**, *414*, 125505.
(131) Rahman, M. A.; Rahman, M. M.; Bahar, M.; Sanderson, P.; Lamb, D. Transformation of Antimonate at the Biochar−Solution Interface. *ACS EST Water* **2021**, *1*, 2029−2036.


https://doi.org/10.1021/acsomega.1c04129
*ACS Omega* 2022, 7, 101−117